Title

Synergic activity of FGFR2 and MEK inhibitors in the treatment of FGFR2-amplified cancers of unknown primary

Authors

*Andrea Cavazzoni[1#], Irene Salamon[2#], Claudia Fumarola[1#], Giulia Gallerani[2], Noemi Laprovitera[3], Francesco Gelsomino[3], Mattia Riefolo[2,3], Karim Rihawi[3], Elisa Porcellini[2], Tania Rossi[4], Martina Mazzeschi[2], Maria Naddeo[2,3], Salvatore Serravalle[3], Elisabetta Broseghini[2], Federico Agostinis[5$], Gabriele Sales[5], Olivier Deas[6], Giorgio Durante[2], Mattia Lauriola[2], Ingrid Garajova[7], George A. Calin[8], Massimiliano Bonafè[2,3], Antonia D'Errico[2,3], Pier Giorgio Petronini[1], Stefano Cairo[6§], Andrea Ardizzoni[2,3] and Manuela Ferracin[2,3]**

1 Department of Medicine and Surgery, University of Parma, Parma (Italy)
2 Department of Medical and Surgical Sciences (DIMEC), University of Bologna, Bologna, Italy
3 IRCCS, Azienda Ospedaliero-Universitaria di Bologna, Bologna, Italy.
4 Istituto Scientifico Romagnolo per lo Studio e la Cura dei Tumori (IRST) IRCCS, Meldola (FC) (Italy)
5 Department of Biology, University of Padova, Padua, Italy
6 XenTech, Evry, France
7 Medical Oncology Unit, University Hospital of Parma, Via Gramsci 14, 43126, Parma, Italy
8 Department of Experimental Therapeutics, The University of Texas MD Anderson Cancer Center, Houston, TX 77030, USA

# These authors contributed equally
$ FA is currently an Associate Data Analyst & Data Scientist at Evotec SE (Hamburg, Germany)
§ SC is currently senior global scientific director at Champions Oncology (USA)

*Correspondence: manuela.ferracin@unibo.it

Summary

Patients with cancer of unknown primary (CUP) carry the double burden of an aggressive disease and reduced access to therapies. Experimental models summing up CUP features are pivotal for CUP biology investigation and drug testing. We derived two CUP cell lines (CUP#55 and #96), and corresponding patient-derived xenografts (PDXs), from ascites tumor cells. CUP cell lines and PDXs underwent histological, immune-phenotypical, molecular, and genomic characterization confirming the features of the original tumor. Genetic testing and FISH analysis identified FGFR2 amplification as therapeutic target in tumor tissues and patient-derived models. Drug-screening assays were performed to test the activity of FGFR2 targeting drug BGJ-398 (infigratinib) and the combination treatment with the MEK inhibitor trametinib, which proved to be synergic and exceptionally active, both *in vitro* and *in vivo*. This study brings personalized therapy closer to CUP patients and paves

the way to future applications of personalized medicine for metastatic patients with adverse prognosis.

Keywords
CUP, patient-derived xenografts, genetic test, FGFR2, FGFR2 inhibitor, MEK inhibitor, infigratinib, site-of-origin prediction

Introduction

Metastases develop when tumor cells spread from the primary site to surrounding or distant tissues and are responsible for 90% of cancer-related deaths (Chaffer and Weinberg, 2011). Among metastatic patients, 3-5% show no clinical evidence of a primary site at diagnosis. These cases are classified as cancers of uncertain origin or cancers of unknown primary site (CUPs) or occult primary tumors (Laprovitera et al., 2021a; Varadhachary and Raber, 2014). They are usually diagnosed at a late stage, with patients presenting one or more metastases already at first diagnosis. The identification of tumor primary site is usually obtained by a combination of diagnostic investigations including physical examinations, blood analyses, imaging and immunohistochemical (IHC) testing of the tumor tissue. In CUP patients, these investigations are inconclusive.

International guidelines for tumor treatment are based on primary site indication. Therefore, CUP treatment requires a blind approach, which is very challenging for oncologists. Consequently, CUPs are typically treated with empiric platinum-based chemotherapy regimens, which are usually poorly effective. Indeed, CUP patients have a short life-expectancy (average overall survival 4-9 months, with only 20% surviving more than 1 year) which, unfortunately, did not improve over the last decades. However, these regimens remain empirical since they are mostly based on results of single-arm phase II clinical trials (Briasoulis et al., 2008; Pentheroudakis et al., 2008; Warner et al., 1998) or small phase III trials (Gross-Goupil et al., 2012; Hainsworth et al., 2015; Huebner et al., 2009).

The use of molecular tests based on gene/miRNA expression signatures or methylation profiles to identify the most probable site-of-origin could assist the oncologists in the selection of the best treatment options and potentially improve CUPs outcome (Laprovitera et al., 2021b; Laprovitera et al., 2021c). NCCN guidelines for occult primary tumors recently introduced the recommendation to use NGS genetic testing to guide therapeutic decision (v.2/2023) and suggest 11 different chemotherapy regimens for adenocarcinoma and 9 for squamous histology.

With the advent of personalized medicine, patient management is more and more frequently associated with the identification of specific molecular or genetic features of the tumor upon which therapies could be based to avoid suboptimal treatments. The identification of druggable alterations in CUP tumors could increase the otherwise limited treatment options, as recently demonstrated by Hayashi et al. (Hayashi et al., 2020). Next generation sequencing technologies were applied to the analysis of CUP mutational profile (Clynick et al., 2018; Consortium, 2017; Ross et al., 2015; Varghese and Saltz, 2015; Zehir et al., 2017). Overall, CUPs seem to harbor recognized actionable genetic alterations in nearly 30% of cases (Laprovitera et al., 2021a; Lombardo et al., 2020). Immunotherapy has been scarcely tested on CUP patients: in a study by Gatalica et al. only a fraction of patients presented favorable biomarkers for the use of immune checkpoint inhibitors (Gatalica et al., 2018). Varghese et al. identified the actionable mutations in a dataset of 150 CUPs analyzed with the MSK-IMPACT panel and patients who were treated with targeted therapies, showed clinical benefit and longer survival. A meta-analysis conducted by Ding et al. confirmed a benefit for site-specific therapies only for CUP patients with a stronger primary site prediction (Ding et al., 2022).

However, the knowledge that molecular and genetic testing could provide novel personalized treatments for CUP patients is hampered by the lack of cellular and animal models on which to test potentially effective therapies.
A main limitation in the development of CUP models is posed by the reduced availability of fresh tumor cells, given that the biopsy is frequently entirely dedicated to the diagnostic workup and surgery is rarely an option for these patients. Circulating tumor cells have been tracked in the blood of CUP patients (Laprovitera et al., 2021c) and could be the source of tumor cells for cell lines development; this is true also for ascites fluid, when available. Liquid biopsy tumor cells would have the advantage of being more representative of the overall complexity and heterogeneity of CUP tumors.
Recently, Verginelli et al. described the generation of the first CUP *in vitro* and *in vivo* models from biopsy/surgery tumor tissue, showing how they recapitulate the genetic of the original tumors and present a stem cell-like phenotype. Since tumor cell proliferation in their models was sustained by constitutively activation of the MAPK pathway, they described how the use of MEK1/2 inhibitor, trametinib, strongly reduced cell viability and tumor volume in xenograft models. This is the first study to describe the activation of an oncogenic pathway shared among CUPs, which supported a specific therapeutic intervention.
In this study, we obtained and expanded two patient-derived CUP cell lines from ascites tumor cells, spontaneously growing as spheroids and organoids, and corresponding patient-derived xenografts (PDXs). We obtained the immunophenotypic, molecular and genomic characterization of the tumor and derived models, confirming the recapitulation of the original features. Finally, we performed a drug-screening assay to target actionable genes and identified a combination of drugs with promising antitumor activity, both *in vitro* and *in vivo*.

Results

Establishment of two CUP models from ascites tumor cells: immunophenotypical, genetic and molecular characterization

We generated *in vitro* and *in vivo* CUP models to test tailored experimental pharmacological approaches. CUP patient #55 was diagnosed with multiple lymph node metastases of poorly differentiated adenocarcinoma. Immunohistochemistry (IHC) staining reported the positivity for keratin 7 (K7) and CDX2, weak positivity for keratin 20 (K20) and negativity for neuroendocrine markers (chromogranin, synaptophysin, CD56). CUP patient #96 presented with multiple metastases of poorly differentiated adenocarcinoma with peritoneal carcinosis and multiple sub- and supra-diaphragmatic lymph node metastases. The tumor IHC staining was positive for K7, K20, CDX2, EpCAM and negative for PAX8, p40, GATA3 and calretinin.
Two long-term (more than 10 passages (Janik et al., 2016)) cell lines were obtained isolating cells from ascites fluid of the patients #55 and #96. One month after seeding, cells growing in suspension were visible as spheroid-like structures (**Supplementary Figure 1**). The growth curve of two models was monitored for 10 days using the Incucyte S3 live-cell analysis: 10000 cells of CUP#96 and CUP#55 were seeded and after few hours CUP#96 cells formed large tumoroids and CUP#55 cells

organized as clusters, showing a doubling time of 5 days for both cell lines **(Supplementary figure 2 and 3).**

We generated two PDX models by injecting ascites tumor cells in the interscapular region of immunocompromised mice as described in the Methods section. The two models showed different growth rate, with CUP#96 PDX growing faster than CUP#55 PDX, and with CUP#55 PDX inducing a tumor-intrinsic mild cachexia in the mice (**Supplementary Figure 4**).

Morphology and histology of the cell lines and PDXs recapitulated the features of the primary tumor (**Figure 1A-B**). To verify whether CUP tumor cells presented a stem-cell like phenotype, the two tumoroid cell lines were tested for CD44 and EPCAM immunoreactivity and the expression of stemness genes CD44, NANOG and OCT4 (**Figure2**). The two cell lines express CD44 on their surface, which is more homogeneous for CUP#96 (**Figure 2A**), and both express stemness genes at high levels if compared to a panel of cancer cell lines (**Figure2B**).

We recently developed a predictive microRNA-based test to assign a possible primary site to metastatic cancers, including occult primary tumors. (Laprovitera et al., 2021b). When we applied the predictive algorithms to the two tumors, we obtained a site-of-origin prediction: CUP#55 was predicted to be of biliary tract origin (probability of 93%) and CUP#96 of gastrointestinal tract origin (probability of 99%).

The tumor tissue, circulating cell-free DNA (ccfDNA), cell line and PDX were tested for genetic alterations with a CUP-dedicated, 92-gene custom panel using SureSelect Target Enrichment technology (Agilent Technologies) as described in (Laprovitera et al., 2021c). The summary of all genetic alterations is reported in **Table 1 and 2**. The genetic analysis of CUP#55 confirmed the detection of 5 genetic alterations in all the analyzed samples (bulk tumor DNA, ccfDNA, cell line and PDX): the insertion in the *APC* gene (p.T1556fs*3) and the point mutations in *ARID1A* (p.R1276∗), *ERBB3* (p.S128R), *KEAP1* (p.R135H) and *NTRK1* (p.Q736X). Mutations in ALK, EPHA5, FAT1, KMT2C, MGA, PTPRD (except for p.L970V) and TP53 were detected only in ccfDNA (**Table 1**). As expected, the variant allele fractions (VAFs) were higher in PDX and cell line, thus reflecting the greater tumor purity and the possible selection of tumor subclones. Low frequency mutations in *ZFHX3, RBM10, PTPRT, NF1, MED12, MGA, KDR, KDM5A, GRIN2A, EP300, DOT1L, APC* (p. S887R), were identified in the models but not in other samples. The generic analysis of CUP#96 was conducted on ccfDNA and cell line due to the unavailability of residual tumor sample for this patient. Five genetic alterations were detected in both samples (**Table 2**), including *TP53*, *SMAD*, *KMT2C*, *CTNNB*, with higher VAFs in the cell line compared to ccfDNA. Low-pass Copy Number Analysis on the two cell lines revealed several regions of amplification and deletion, including copy-number amplification in chromosome 10 encompassing *FGFR2* oncogene (**Supplementary Table 1 and 2**).

FGFR2 amplification in CUP#55 and CUP#96 cell lines provides the rationale to target the receptor using a selective inhibitor

FGFR2 genomic alterations are detected in CUPs with a frequency ranging from 3-4% (**Supplementary Figure 5**). The *FGFR2* amplification in our two models was confirmed with Fluorescence In Situ Hybridization (FISH) and droplet digital PCR (ddPCR). FISH demonstrated the different nature of *FGFR2* amplification: CUP#96 displays an extrachromosomal DNA amplification in the form of double minutes; CUP#55 shows a homogeneously staining region (HSR) associated

with *FGFR2* chromosomal amplification (**Figure 3A**). The copy number variation (CNV) of *FGFR2* gene was confirmed by ddPCR using a probe-based assay in circulating cell-free (ccfDNA), cell line and PDX of both patients (**Figure 3B**). *FGFR2* copy number (CN) in tumor DNA is about 90 for CUP#55, and >400 for CUP#96.

Consistent with the CN amplification, FGFR2 gene expression is increased in both cell lines (**Figure 3C)**. We monitored the FGFR2 isoform expressed by the cell lines and found that both cell lines express the epithelial FGFR2 IIIb isoform and the mesenchymal FGFR2 IIIc isoform (**Supplementary Figure 6**). Western blot analysis confirmed that CUP#96 cells express higher levels of total FGFR2 protein compared to CUP#55 cells. Interestingly, in both models the FGFR2 appears constitutively phosphorylated (**Figure 3D**). Notably, the FGFR2 phosphorylation/expression is higher than in a reference FGFR2 positive cell line (H1581), derived from a lung adenocarcinoma with FGFR1 and FGFR2 amplification (SenthilKumar et al., 2020) (**Figure 3C-D**). FGFR2 gene amplification and activation in CUP#55 and CUP#96 cells provided the rationale for the pharmacological targeting of this receptor for therapeutic intervention.

Simultaneous inhibition of FGFR2/AKT and MAPK pathways by BGJ398 and trametinib, respectively, induces synergistic anti-proliferative and pro-apoptotic effects in CUP models *in vitro*

We preliminarily tested a panel of multikinase inhibitors (BJ398, dovitinib, ponatinib) for their effect on CUP#55 cell vitality. BGJ398 (infigratinib), a selective inhibitor of the FGFR family, demonstrated stronger antitumor activity (**Supplementary figure 7**), and it was selected for further testing in CUP#55 and CUP#96 cells. In CUP#55, the treatment with this drug at different concentrations (range 0.5-2.5 µM) inhibited FGFR2 phosphorylation and the downstream AKT/mTOR/p70S6K signaling (**Figure 4A**). In contrast, ERK1/2 remained phosphorylated even at the highest BGJ398 concentration. CUP#55 cells were sensitive to BGJ398 treatment, although a complete inhibition of their viability/proliferation was not achieved even at 1 µM BGJ398 concentration (**Figure 4C**), suggesting that FGFR-independent mechanisms sustain the activation of the MAPK pathway and contribute to cell growth in this model. These results prompted us to test whether targeting the MAPK pathway with trametinib, a highly specific inhibitor of MEK1/2 proteins, might improve the efficacy of BGJ398 treatment. The drug combination inhibited both the AKT and MAPK pathways almost completely (**Figure 4B**), thereby evidencing a highly significant synergistic inhibition of cell proliferation, as indicated by the comparison with the theoretical interaction curve in the Bliss experimental model ($p<0.001$) (**Figure 4C**). Interestingly, even if the single treatment with either BGJ398 or trametinib did not induce cell death in CUP#55 cells, their combination had a cytotoxic effect, as demonstrated by fluorescence microscopy analysis of Hoechst 33342/PI-stained cells; the morphology of the stained nuclei suggested that the cells died by apoptosis (**Figure 4D**, **Supplemental Figure 8**).

Then, we analyzed the effects of FGFR2 inhibition by BGJ398 treatment in CUP#96 cells. Inhibition of FGFR2 phosphorylation by BGJ398 treatment resulted in the downregulation of phosphorylated forms of AKT, p70S6K, and ERK1/2 levels, suggesting that both AKT and MAPK pathways are downstream of FGFR2 in this cell model (**Figure 5A**). We tested the combination of BGJ398 with trametinib also in these cells and found that it produced a remarkable synergistic inhibition of cell proliferation **(Figure 5B-C**), comparable to that observed in CUP#55 cells, suggesting that trametinib

can provide a more effective inhibition of the MAPK pathway leading to suppression of cell growth also in this cell model. Of note, BGJ398 and trametinib alone were cytotoxic in CUP#96 cells, an effect that was further enhanced by the combined treatment (**Figure 5D**).
Altogether, these findings indicate that trametinib significantly improves the efficacy of FGFR2 targeting in FGFR2-amplified CUP cells.

***In vivo* synergic activity of FGFR2 and MEK inhibitors**

We tested whether *in vitro* findings on FGFR2 and MEK inhibitors synergic activity could be recapitulated in CUP#55 and CUP#96 PDX models *in vivo*.
Mice were treated with control vehicle, BGJ398 (15 mg/kg), trametinib (0.6 mg/kg), and trametinib/BGJ398 combination (N=5 per group). The scheme of different treatments is reported in **Figure 6 A** and **B**, and the effect of different drugs was evaluated measuring the tumor volume. Single drug (BGJ398 or trametinib) treatment significantly reduced the tumor volume in PDX#96 but not in PDX#55 xenografts mice if compared to tumors of mice treated with vehicle. However, the combination of trametinib and BGJ398 resulted more effective than the single treatments in both PDX models, as demonstrated by the dramatic reduction of the tumor volume (**Figure 6A, B**). CUP#55 PDX mice suffered from tumor-induced cachexia and for this reason they were sacrificed after 2 weeks of treatment. CUP#96 PDX mice were treated for up to 33 days with the combination and were sacrificed at 6 weeks.

Discussion

Treatment choice for cancer of unknown primary patients is always challenging due to the inconclusiveness of classical diagnostic investigations in tumor type identification. In this scenario, therapy can be based on empirical approaches, molecular predictions of the primary site, the clinical assessment of the similarity with other known tumor types or more recently, on personalized genetic approaches. Indeed, the combination of molecular and genetic investigations can help the treating clinicians to define the most probable site-of-origin or potential druggable mutations and use this information to choose the best therapeutic strategies.

CUP therapeutic choice has been also hampered by the lack of CUP models on which to test novel therapeutic approaches or investigate the biology of this aggressive disease. Verginelli et al. described the first CUP experimental models adopted to investigate molecular and genetic alterations of the disease (Verginelli et al., 2021). The authors demonstrated that CUP models present a specific stem-cell like phenotype and tested for the first time their sensitivity to MEK inhibitors. Here, we described two *in vitro* and *in vivo* models we derived from ascites circulating tumors cells (CTCs) of CUP patients, named CUP#55 and CUP#96. Using a CTC-optimized protocol, we established two long-term cell cultures spontaneously growing as spheroids/tumoroids and expressing stem-cell markers. The ascites CTCs were engrafted into mice to generate two patients derived xenografts, which recapitulated the characteristics of the original tumor. The genetic analyses, performed on tumor tissues and models, revealed that the two models shared the *FGFR2* amplification as main genetic alteration, although of a different nature. *FGFR2* amplification is

reported in several solid tumors, including gastric cancer and breast cancer (Katoh, 2008), while its translocation is a recurrent feature in cholangiocarcinoma (Smyth et al., 2017).

FGFR2 amplification is associated with increased levels of the protein and its aberrant phosphorylation leads to the activation of downstream pathways, including MAPK-ERK signaling (Babina and Turner, 2017), which in turn accelerate cell proliferation. Since FGFR2 amplification is a druggable target (Babina and Turner, 2017) we investigated the extent of CUP tumors FGFR2 dependency. The treatment with BGJ398 (infigratinib), a pan-FGFR inhibitor, demonstrated the effectiveness of this target therapy in reducing AKT activation, but did not completely prevent ERK1/2 phosphorylation, which remained active through alternative mechanisms. This finding suggests that FGFR2 targeting in FGFR2-amplified CUPs might not be sufficient to halt tumor growth, due to the concomitant activation of alternative survival/proliferation pathways. Therefore, we investigated the effect of the combined use of trametinib, a MAPK pathway inhibitor selective for MEK1/2. MAPK is a pathway that is frequently activated in CUPs (Krikelis et al., 2012), where its activation correlates with worse prognosis. Interestingly, the combined treatment with FGFR2 and MEK inhibitors generated a remarkable synergistic effect, reducing cell growth and viability in both cell models. To validate the results in a preclinical model, the corresponding PDXs were treated with the drug combination and the effect was a drastic reduction of the tumor size if compared with single treatments. The treatment combination was well tolerated by the CUP#96 model but aggravated the mice frailty in CUP#55 model, which already presented signed of tumor-induced cachexia.

In the last years, pemigatinib and infigratinib, both orally active agents targeting FGFR1-4, have received an accelerated approval by US Food and Drug Administration (FDA) for the treatment of adult patients with previously treated and unresectable or metastatic cholangiocarcinoma harboring *FGFR2* fusion or other rearrangement. Based on some concerns, European agency (EMA) granted approval with the same indication only for pemigatinib. Likewise, erdafitinib, an orally active small potent TKI of FGFR1–4, was granted accelerated approval for patients with locally advanced or metastatic urothelial carcinoma, with susceptible FGFR3 or FGFR2 genetic alterations.

FGFR inhibitors have also been largely tested in gastric cancer patients with less enthusiastic results so far. However, positive results from a phase II trial have been reported by using bemarituzumab in addition to chemotherapy as first line treatment for metastatic HER-2 negative gastroesophageal cancer patients with FGFR2b hyperexpression or *FGFR2* gene amplification (Wainberg et al., 2022). As such, several phase II and phase III trials currently ongoing. Other new compounds, alone or in combination with other agents, are under investigation for the treatment of multiple solid tumors carrying FGFR alterations. Our results suggest that the combination of FGFR and MEK inhibitors could be a potential strategy to improve clinical outcomes in cancer patients carrying FGFR gene alterations. This means that co-targeting cross-talking pathways may potentiate FGFR inhibition, and improve the therapeutic benefit, as we have demonstrated with the MEK inhibitor trametinib.

Based on the evidence that MEK inhibition in KRAS-mutant lung cancer leads to compensatory MAPK pathway reactivation through FGFR1, combining trametinib with FGFR1-specific inhibitors encapsulated in nanoparticles allowed to efficaciously inhibit growth and proliferation in KRAS-

mutant/FGFR compensatory cancer cells (Izawa-Ishiguro et al., 2022). In this regard, a phase 1/2 study is recruiting patients with advanced cancer of any tumor type (Part 1) or non-small cell lung cancer (NSCLC) with a confirmed KRAS mutation (Part 2) to determine the recommended dose and antitumor activity of futibatinib (a selective, irreversible FGFR1-4 inhibitor) in combination with binimetinib, a known MEK inhibitor (NCT04965818).

Our study contributes to fill the gap in CUP model availability, through the generation of two human cell lines and corresponding PDXs. We demonstrated how the molecular characterization and genetic profile of the tumor can provide information to predict the most probable site-of-origin and identify druggable targets. In fact, the development of models that mirror the phenotype and genotype of human tumors *in vitro* and *in vivo*, has become a helpful tool for drug screening, particularly to assess new therapeutic combinations that could be translated to patients with the same genetic alterations or molecular features. Finally, the availability of CUP models for future studies will contribute to deepen our knowledge on the mechanisms at the base of CUP high proliferative and metastatic potential and still mysterious biology.

Acknowledgments

The research leading to these results has received funding from AIRC under IG 2021 - ID. 25789 project – P.I. Ferracin Manuela. MF lab is supported by Pallotti funds and Fondazione del Monte.

Author contributions

Conceptualization AC, CF and MF; Methodology, EP, GS, OD and SC; Investigation AC, CF, IS, NL, GG, MR, FG, MN, KR, TR, MM, SS, EB, FA and GD; Resources, ML, IG, AD, PGP, AA and MF; Writing-Original Draft AC, IS, CF and MF; Writing-Review & Editing, GC, MB, AA and MF; Funding Acquisition, MF

Declaration of interests

Francesco Gelsomino received personal fees from AstraZeneca and honoraria for advisory board participation from Eli-Lilly.

Figure titles and legends

Figure 1. A) Immunophenotypic characterization of tumor tissues, cell lines and PDX of CUP#55. Hematoxylin-eosin (HE), keratin7 (K7) and keratin20 (K20) IHC staining was reported for tumor tissue, cell lines and PDX in CUP#55 model (40x). The staining showed that cell line and PDX models recapitulated the histology of the tumor tissue. **B) Immunophenotypic characterization of tumor tissues, cell lines and PDX of CUP#96.** Hematoxylin-eosin (HE), keratin7 (K7) and keratin20 (K20) IHC staining was reported for tumor tissue, cell lines and PDX in CUP#96 model (40x). CUP#96 cell line grows forming tumoroid structures. The staining showed that cell line and PDX models recapitulated the histology of the tumor tissue.

Figure 2. CUP models characterization. A) Immunophenotypic analysis of CUP #55 and #96 cell lines demonstrating the expression of cancer stem cell markers CD44 and EPCAM. Staining: nucleus (DAPI, blue), CD44 and EPCAM (green). **B)** Gene expression analysis of stemness genes in CUP#55 and CUP#96. Bars represent the ratio between the gene copies and the reference HPRT copies assessed by ddPCR. The expression in CUP cell lines was compared to other cancer cell lines from lung and melanoma origin.

Figure 3. FGFR2 amplification in CUP models. A) FISH analysis shows the different nature of FGFR2 amplification in the two CUP cell models: double minutes for CUP#96 and HSR for CUP#55; FGFR2 gene probe is in red, Chr10 centromere probe in green, nucleus in blue. **B)** Copy number variation (CNV) analysis of FGFR2 gene detected by ddPCR using a probe-based assay. **C)** FGFR2 gene expression in the two amplified models and a control not amplified cell line. Bars represent the ratio between the gene copies and the reference HPRT copies assessed by ddPCR. **D)** Evaluation by western blot analysis of total and phosphorylated forms of FGFR2 in CUP#55 and #96, compared to the H1581 NSCLC cell line.

Figure 4. ***In vitro* FGFR2 targeting and synergic activity of FGFR2 and MEK inhibitors in CUP#55. A)** CUP#55 cells were treated with BGJ398 at the indicated concentrations; after 24h, protein extracts were analyzed by Western blotting for the indicated proteins. The results are representative of two independent experiments; B**)** CUP#55 cells were incubated with BGJ398 1µM, trametinib 100 nM, or the combination; after 24h, protein extracts were analyzed by Western blotting for the indicated proteins. The results are representative of two independent experiments; **C)** CUP#55 cells were treated with increasing concentrations of BGJ398 in combination with trametinib 100 nM. After 96h, cell proliferation was assessed by MTS assay. The data are expressed as percent inhibition *vs.* control. The asterisks indicate the statistical significance *vs.* the corresponding points of the Bliss Theoretical curve. The results are representative of three independent experiments; **D)** CUP#55 cells were incubated with BGJ398 1µM and/or trametinib 100nM; after 96h, the percentage of cell death was evaluated by fluorescence microscopy after Hoechst 33342/PI staining. The data are mean values ±SD of three independent experiments. **$p<0.01$, ***$p<0.001$.

Figure 5. ***In vitro* FGFR2 targeting and synergic activity of FGFR2 and MEK inhibitors in CUP#96. A)** CUP#96 cells were treated with BGJ398 at the indicated concentrations; after 24h, protein extracts were analyzed by Western blotting for the indicated proteins. The results are representative of two independent experiments; **B)** CUP#96 cells were incubated with BGJ398 100nM, trametinib 10 nM or the combination; after 24h, protein extracts were analyzed by Western blotting for the indicated proteins. The results are representative of two independent experiments; **C)** CUP#96 cells were treated with increasing concentrations of BGJ398 in combination with trametinib 10 nM. After 96h, cell proliferation was assessed by MTS assay. The data are expressed as percent inhibition *vs.* control. The asterisks indicate the statistical significance *vs.* the corresponding points of the Bliss Theoretical curve. The results are representative of three independent experiments; **D)** CUP#96 cells were incubated with BGJ398 100 nM and/or trametinib 10 nM; after 96h, the percentage of cell death was evaluated by fluorescence microscopy after Hoechst 33342/PI staining. The data are mean values ±SD of three independent experiments. *p<0.05; **p<0.01, ***p<0.001, ****p < 0.0001.

Figure 6. *In vivo* activity of FGFR2 and MEK inhibitors. *In vivo* treatment of **A)** PDX#96 PDXs and **B)** PDX#55 PDXs. The timeline shows the day of tumor volume measurement, and the color bars represent the scheme of each treatment. The line graph shows that the combination of trametinib+BGJ398 treatments (purple) is more effective than the single ones (trametinib in red and BGJ398 in blue) in both PDX models. N=5 mice per group. *p<0.05, **p<0.01, ***p<0.001, ****p<0.0001.

Tables with titles and legends

Table 1. Genetic alterations detected in CUP#55 patient-derived tissues and models

Gene	coding change	aminoacidic change	tumor FFPE	ccfDNA at diagnosis	ccfDNA at disease progression	cell line	PDX Passage1	predicted as pathogenic*
ALK	c.A1301G	p.K434R	not detected	not detected	7.0%	not detected	not detected	no
APC	4607insA	p.T1556fs*3	9.8%	22.6%	29.9%	100.0%	95.0%	ND
APC	c.A2659C	p.S887R	not detected	not detected	not detected	43.2%	not detected	yes
ARID1A	c.C3826T	p.R1276X	8.9%	28.5%	22.8%	53.0%	19.8%	yes
CREBBP	c.T1448C	p.L483P	not detected	not detected	not detected	not detected	21.7%	ND
DOT1L	c.A1193C	p.K398T	not detected	not detected	not detected	38.2%	not detected	yes
EP300	c.A7118C	p.N2373T	not detected	not detected	not detected	not detected	32.2%	no
EPHA5	c.A1417C	p.T473P	not detected	not detected	8.3%	not detected	not detected	no
ERBB3	c.C384A	p.S128R	9.8%	20.7%	20.4%	41.09%	48.60%	yes
ERBB4	c.T343A	p.Y115N	not detected	not detected	not detected	not detected	33.8%	yes
FAT1	c.A2084C	p.N695T	not detected	not detected	2.6%	not detected	not detected	no
GRIN2A	c.A4064C	p.K1355T	not detected	not detected	not detected	not detected	22.3%	no
KDM5A	c.T3547C	p.W1183R	not detected	not detected	not detected	not detected	22.2%	yes
KDR	c.A981C	p.K327N	not detected	not detected	not detected	not detected	27.9%	ND
KEAP1	c.G404A	p.R135H	9.0%	22.6%	19.5%	51.8%	44.0%	yes
KMT2C	c.C2459T	p.T820I	not detected	1.1%	1.1%	not detected	not detected	yes
KMT2C	c.C1013T	p.S338L	not detected	5.5%	4.3%	not detected	not detected	no
KMT2C	c.C2689T	p.R897X	not detected	not detected	1.4%	not detected	not detected	yes
KMT2C	c.C2228T	p.P743L	not detected	not detected	1.6%	not detected	not detected	no
MED12	c.A688C	p.I230L	not detected	not detected	not detected	not detected	25.0%	no
MGA	c.A395C	p.N132T	not detected	not detected	not detected	not detected	30.5%	yes
MGA	c.T4004C	p.L1335P	not detected	not detected	1.6%	not detected	not detected	ND

NF1	c.A6083G	p.K2028R	not detected	not detected	not detected	not detected	25.4%	yes
NTRK1	c.C2206T	p.Q736X	8.3%	26.0%	22.3%	32.6%	44.7%	yes
PALB2	C2419T	p.P807S	9.0%	19.1%	16.6%	not detected	47.4%	no
PTPRD	c.T2908G	p.L970V	not detected	5.1%	3.5%	not detected	47.7%	yes
PTPRD	c.A3117C	p.Q1039H	not detected	not detected	6.8%	not detected	not detected	yes
PTPRT	c.T479C	p.F160S	not detected	not detected	not detected	not detected	33.8%	no
RBM10	c.A2024G	p.K675R	not detected	not detected	not detected	not detected	41.7%	no
TP53	c.C9G	p.C3W	not detected	1.2%	not detected	not detected	not detected	yes
TP53	c.A355G	p.I119V	not detected	1.7%	not detected	not detected	not detected	yes
TP53	c.G315C	p.M105I	not detected	1.8%	not detected	not detected	not detected	yes
TP53	c.T316C	p.C106R	not detected	2.1%	not detected	not detected	not detected	yes
ZFHX3	c.A1604C	p.E535A	not detected	not detected	not detected	not detected	27.5%	no
ZFHX3	c.A7529G	p.Q2510R	not detected	not detected	not detected	not detected	39.7%	no

*variants were considered pathogenic when more than 50% of the 8 predictors (SIFT, Polyphen2 HVAR, LRT, Mutation Taster, Mutation Assessor, FATHMM, CADD and VEST) considered the alteration as pathogenic/damaging/deleterious/harmful. ND= not defined

Table 2. Genetic alterations detected in CUP#96 patient-derived tissues and models

Gene	coding change	aminoacidic change	CUP#96 cell line	ccfDNA at diagnosis	predicted as pathogenic *
PIK3C2G	c.G1813A	p.V605I	100.00%	48.35%	no
TP53	c.G418A	p.V140M	100.00%	49.34%	yes
SMAD4	c.A1610G	p.D537G	100.00%	44.23%	yes
KMT2C	c.G943A	p.G315S	4.58%	5.31%	yes
CTNNB1	c.C110T	p.S37F	55.10%	22.39%	yes
KMT2C	c.A2725G	p.R909G	-	6.48%	yes
KMT2C	c.C3274T	p.R1092X	-	5.28%	yes
KMT2C	c.C1013T	p.S338L	-	4.57%	no

KMT2C	c.G944A	p.G315D	-	3.09%	yes

*variants were considered pathogenic when more than 50% of the 8 predictors (SIFT, Polyphen2 HVAR, LRT, Mutation Taster, Mutation Assessor, FATHMM, CADD and VEST) considered the alteration as pathogenic/damaging/deleterious/harmful. ND= not defined

STAR Methods

Cell culture

NSCLC cell lines H1581, A549, H460, H2228, H1299 and SK-MEL-28 were from ATCC (Manassas, VA, USA). Cells were cultured in RPMI-1640 medium (Corning) supplemented with 10% fetal bovine serum (Corning) and maintained under standard cell culture conditions at 37°C in a water-saturated atmosphere of 5% CO_2 in air.

Tumor spheroids growth evaluation

The Incucyte S3 live-cell analysis system (Sartorius, Essen Bioscience) was used for the measurements of spheroid formation and growth. Cells were seeded in a 96-well round bottom ultra-low attachment plate, centrifuged, and placed into the Incucyte live-cell analysis system. The acquisition was scheduled every 6 hours with a 4x objective. Acquired images were analyzed generating a mask that cover the brightfield object area and measuring the mask size over time using the Incucyte S3 DF Brightfield analysis automated software algorithm. Monitoring the size and the tumor spheroids morphology at different time point, the software created a growth curve.

Patients and ascites CTC isolation

Two patients with a confirmed diagnosis of cancer of unknown primary based on ESMO criteria (CUP#55 and CUP#96) were enrolled in this study at the Oncology Unit of IRCCS Azienda Ospedaliero-Universitaria di Bologna (Bologna, Italy). The study was approved by the local ethical committee (Comitato Etico Indipendente dell'Azienda Ospedaliero-Universitaria di Bologna, Policlinico S.Orsola Malpighi) with protocol number EM435-2022_130/2016/U/Tess/AOUBo. All subjects provided a written informed consent to the study participation.

About 100 ml of ascites from both patients were collected and immediately processed. Ascites samples were centrifuged at 600 g for 10 minutes at 4°C and the obtained pellet was treated with 10 ml red blood cell lysis buffer (Miltenyi Biotec) for 15 minutes at room temperature. Then, 10 ml of specific culture medium (DMEM/F12 50:50, 2 mM glutamine, 5% Horse serum, hydrocortisone 1 ug/ml, insuline 10 µg/ml, 1X PEN/STREP, EGF 10 ng/ml) was added and centrifuged at 600 g for 10 minutes. The cells were plated in T25 flask with 5 ml of medium in humidified 37 °C/5% CO_2 incubator. Medium was changed every 3–4 days. After 10 days, tumor cells begun to grow as tumoroids (CUP#96) and spheroids (CUP#55).

Organoids and aggregates were propagated in 24 well-plates to monitor growth and every 3-4 days splitted 1:2. Long-term CTC cell lines were established: i.e. the cell lines were still viable after thawing cycle and showed a stable growth in medium without supplement (Kodack et al., 2017).

Pathological and immunofluorescence analysis

Cell lines, human and PDX tumor tissues were fixed in 4% paraformaldehyde for 20 minutes, embedded in paraffin and frozen at -20°C for optimal cutting. Sections of 4 µm were mounted on positively charged microscope slides. Sections were deparaffinized in xylene and rehydrated in graded alcohol. Antigen enhancement was done by incubating the sections in Concentrated Antigen Retrival Solution Citra Plus (BioGenex #HK080-5K) (1:10) as recommended by the manufacturer

and blocked with Ventana Antibody Diluent with Casein (Roche-Ventana) for 30 minutes. For immunohistochemistry: Rabbit Monoclonal Primary Antibody Cytokeratin 7 (SP52) (Roche-Ventana) and Rabbit Monoclonal Primary Antibody Cytokeratin 20 (SP33) (Roche-Ventana), were used at 1:2 dilution for cell lines, human and PDX tumor tissues staining.

For immunofluorescence experiment: Mouse Monoclonal Primary Antibody CD44 (or HCAM) sc-7297 (SantaCruz) 1:100 dilution and Mouse Monoclonal Primary Antibody EpCAM FITC (REA764) (Miltenyi) 1:100 dilution was used for cell lines staining. All the antibodies were incubated overnight at 4°C. AbCAM Goat Anti-Rabbit IgG H&L (DyLight® 594) (ab96885) and Donkey Anti-Mouse IgG H&L (DyLight® 488) (ab96875) labeled secondary antibodies were used at 1:100 dilution and incubated 1h. Nuclei were counterstained with 1 µg/mL of Hoechst 33342 (Life Technologies). Confocal images were acquired on Nikon A1 confocal laser scanning microscope, equipped with a 60X, 1.4 NA objective and with 405, 488 nm laser lines.

Genetic analysis

We used a custom 1.2-Mb SureSelect capture bait library (Agilent Technologies, Santa Clara, CA, United States) for the target enrichment of 92 genes (panel description in (Laprovitera et al., 2021c)). Briefly, libraries were prepared using 50 ng of gDNA input following SureSelectXT HS/SureSelectXT Low Input Target Enrichment with Pre-Capture Pooling protocol (G9702-90005, v. A0, June 2019, Agilent Technologies) and sequenced on NextSeq 500 (Illumina) platform using High Output 2 × 75-bp flow cells. Variant calling and paired analyses (tumor vs. normal) were performed using SureCall software (v. 4.2), applying a filter for tumor/normal tissue/models at 5% and for ccfDNA at 1%. Variants were annotated using ANNOVAR (Wang et al., 2010) and filtered to keep somatic exonic non-synonymous single-nucleotide variants (SNVs), insertions, deletions, multiple nucleotide variants, or long deletions not detected in the normal sample that presented an allele frequency in Non-Finnish European (NFE) population lower than 0.5% (Genome Aggregation Database, GnomAD; Karczewski et al., 2020) and a coverage higher than 100. Bioinformatic pathogenicity prediction, reported in Tables 1 and 2 of the identified variants was performed consulting the prediction score/outcome of 8 prediction models: SIFT (Sort Intolerated From Tolerated; Vaser et al., 2016), Polyphen2 HVAR (Polymorphism Phenotyping v2; Adzhubei et al., 2010), LRT (Likelihood Ratio Test; Chun and Fay, 2009), Mutation Taster (Schwarz et al., 2014), Mutation Assessor (Reva et al., 2011), FATHMM (Functional Analysis Through Hidden Markov Model; Shihab et al., 2013), CADD (Combined Annotation Dependent Depletion; Kircher et al., 2014), and VEST (Variant Effect Scoring Tool; Douville et al., 2016). Variants were considered pathogenic when more than 50% of the above-mentioned predictors indicated it as pathogenic/damaging/deleterious/harmful.

Gene expression analysis

RNA was extracted from 2 CUP cell lines and 5 cancer cell lines (A549, H2228, H460, H1299, SKMEL). 500ng of RNA for each cell line were reverse-transcribed to cDNA using iSRCIPT cDNA Synthesis Kit (Cat. No. 1708891 Bio-Rad, USA). The expression of CD44, NANOG, OCT4, and FGFR2 was quantified using the QX200 Droplet Digital PCR system (Bio-Rad, Hercules, CA, USA). Bio-Rad EvaGreen protocol for gene expression quantification was used to quantify the gene copies per ng of cDNA by

QuantaSoft Analysis software (Bio-Rad, Hercules, CA, USA). Gene/HPRT (reference gene) ratio was used to normalize the gene expression. The primers used for the gene expression analysis are the following:
CD44 Fw: ATGAGGGATATCGCCAAACA
CD44 Rw: GGTGTTGTCCTTCCTTGCAT
NANOG Fw: TTTGTGGGCCTGAAGAAAACT
NANOG Rw: AGGGCTGTCCTGAATAAGCAG
OCT4 Fw: GGGTTCTATTTGGGAAGGTAT
OCT4 Rw: TTCATTGTTGTCAGCTTCCT
FGFR2 Fw: CAGGGGTCTCCGAGTATGAA
FGFR2 Rw: TCCTTGGGCTTGTCTTTGTC
HPRT Fw: TGACACTGGCAAAACAATGCA
HPRT Rw: GGTCCTTTTCACCAGCAAGCT

Fluorescence In-Situ Hybridization (FISH)
FISH analysis was performed on fixed CUP#55 and CUP#96 interphase nuclei and metaphases. Two Empire Genomics probes (Empire Genomics, Buffalo, NY) were employed following the manufacturer's protocol. Specifically, the FGFR2 gene probe (orange) maps on chr:10q26.13 and the CEP10 probe maps to the centromeric region of Chromosome 10. CUP#55 and CUP#96 cells were counterstained with 40,6-diamidino-2-phenylindole (DAPI) for nuclear detection. Analysis was performed using Olympus BX53 microscopy equipped with the appropriate filter sets and CytoVision software (Leica Biosystems, Nussloch, Germany).

Detection of *FGFR2* amplification
Total DNA was extracted from CUP#55 and CUP#96 cell lines and PDXs using QIAamp DNA Mini Kit (Cat. No. 5130450, Qiagen). Cell free DNA was extracted from 1mL plasma with Maxwell RSC ccfDNA Plasma Kit (Cat No: AS1480, Promega). Tumor DNA was extracted using the QIAamp DNA FFPE Tissue Kit (Cat No: 56404, Qiagen, Hilden, Germany). To quantify the copy number of FGFR2 in all samples, a probe-based droplet digital PCR assay was used. RPP30 was tested as reference gene for diploid copy number. RPP30 probe (dHsaCP2500350, Bio-Rad) was labeled with HEX, and FGFR2 probe (dHsaCB2500320) was labeled with FAM. Droplet digital PCR was performed with the QX200 Droplet Digital PCR system (Bio-Rad, USA) as described in (Laprovitera et al., 2021c). FGFR2 gene copy number was calculated by QuantaSoft Analysis software (Bio-Rad, Hercules, CA, USA) as FGFR2/RPP30 ratio.

Cell Viability and Drug response assays
Cell viability/proliferation was evaluated by a CellTiter-Glo 96 Aqueous One solution Assay (Promega). Cell death was analyzed by fluorescence microscopy after staining with Hoechst 3342 and Propidium Iodide (PI) (Fumarola et al., 2005). BGJ398 (infigratinib) and trametinib (mekinist) were purchased from Selleckchem (Houston, TX), and dissolved in DMSO. DMSO concentration never exceeded 0.1% (v/v); equal amounts of the solvent were added to control cells. The effect of the drug combination was evaluated using the Bliss interaction model (La Monica et al., 2009).

Briefly, a theoretical dose-response curve was calculated for combined inhibition using the equation of Bliss = EA + EB-EA∗EB, where EA and EB are the percent of inhibition *vs* control obtained by BGJ398 (A) and trametinib (B) alone and the E Bliss is the percent of inhibition that would be expected if the combination was exactly additive. If the combination effect is higher than the expected Bliss equation value, the interaction is synergistic, while if the effect is lower, the interaction is antagonistic. Otherwise, the effect is additive and there is no interaction between the drugs.

Western blotting

For Western Blot analysis, $8x10^5$ cells from CUP#55 or CUP#96 were seeded in 6 well-plates in complete culture medium. At the end of the treatments, the cells were harvested and centrifuged. The procedures for protein extraction, solubilization, and protein analysis by western blotting are described elsewhere (Cavazzoni et al., 2008). Antibodies against p-FGFR (#3471), FGFR2 (#11835), p-ERK1/2$^{Thr202/Tyr204}$ (#4370), ERK1/2 (#4695), p-AKT^{Ser473} (#9271), AKT (#9272), p-P70S6K^{Thr389} (#9205), P70S6K (#9202) were from Cell Signaling Technology, Incorporated (Danvers, MA); anti-β-actin (clone B11V08) was from BioVision (Milpitas, CA). Horseradish peroxidase-conjugated secondary antibodies and the chemiluminescence system were from Millipore (Millipore, MA). Reagents for electrophoresis and blotting analysis were from BIO-RAD Laboratories (Hercules, CA). The chemiluminescent signal was acquired by C-DiGit R Blot Scanner and the bands were quantified by Image StudioTMSoftware, LI-COR Biotechnology (Lincoln, NE).

Growth of CUP tumors in immunocompromised mice

PDX studies were run at XenTech in compliance with authorization n. APAFIS#30365-2021012215599431 v1 conferred from the French Ministry of Agriculture and Food. The authorization to use animals in the CERFE facility (Evry-Courcouronne, France) was obtained by The Direction Départementale de la Protection des Populations, Ministère de l'Agriculture et de l'Alimentation, France "Direction of the Veterinarian Services, Ministry of Agriculture and Food, France" (agreement No. D-91-228-107).

An approximate number of 3-4000 cells or 30-40 organoids were resuspended in 100 µl of culture medium, diluted 1:1 in matrigel and grafted in the interscapular region of NOD/Scid-IL2Rγ-/- (NSG) or NOD/Shi-scid/IL-2Rγnull (NOG) mice. Tumor fragments were sampled from the resected tumor, minced on ice and immediately placed in MACS Tissue Storage Solution (Miltenyi Biotech) and transferred to the animal facility, fragmented and grafted in the interscapular region of Athymic Nude-Foxn1nu mice. Mice were monitored twice weekly for signs of tumor growth. Tumor growth from first implantation occurred in 135 days for CUP#55 and 40 days for CUP#96. Growing tumors were serially transplanted onto recipient mice and the fragments of the tumor harvested for IHC analysis, DNA and RNA extraction. To immortalize each PDX, vials of tumor fragments at different passages were placed in 90% FCS/10% DMSO or glycerol, and stored at -150°C.

***In vivo* treatments**

Treatment efficacy study on each PDX were run as follows. Tumor fragments of the same passage were transplanted subcutaneously onto 3-24 mice (donor mice). When the tumors reached 700 to

1764 mm3, donor mice were sacrificed, and tumors were cut into fragments measuring approximately 20 mm3. Mice aged 8 to 11 weeks were anaesthetized with 100 mg/kg ketamine hydrochloride and 10 mg/kg xylazine, and one tumor fragment was placed in the interscapular fat pad. On the day of enrollment in the study mice with tumor volume ranging 60 to 200 mm3 were randomly attributed to the different groups:

Gr.	N	**1st Testing Agent**					**2nd Testing Agent**				
		Agent	Dose mg/kg	Route	Volume ml/kg	Schedule	Agent	Dose mg/kg	Route	Volume ml/kg	Schedule
1	5	Vehicle 1	-	PO	10	qd	Vehicle 2	-	PO	10	qd
2	5	trametinib	0.6*	PO	10	qd	-	-	-	-	-
3	5	-	-	-	-	-	BGJ398	15*	PO	10	qd
4	5	trametinib	0.6	PO	10	qd	BGJ398	15	PO	10	qd

Legend: PO= per os; qd= once daily

From day 12 to day 14 half dose was administered due to body weight loss.

Trametinib was purchased at Carbosynth and suspended in 10% DMSO; 40% PEG300; 5% Tween-80; 45% NaCl 0.9% for administration; BGJ398 (infigratinib) was purchased at MedChem Express and diluted in 50% Acetic acid/acetate buffer / 50% PEG300 for administration. Tumor volume was evaluated by measuring tumor diameters with a caliper, three times a week during the treatment period (from D0 to D27); all animals were weighted, and tumor size measured the same day. During the whole experimental period, animals were monitored every day for physical appearance, behavior, and clinical changes.

Supplemental titles and legends

Supplemental Figure 1. Brightfield representative images of cultured cell lines growing as in suspension 3D-structures. CUP cell lines display specific *in vitro* growth characteristics. CUP#96 grow as tightly compact tumoroids and require trypsinization for passaging. CUP#55 forms loosely aggregated and weakly tight strands requiring only gentle mechanichal dissociation for disgregation. All established cell lines remain viable after freezing and thawing at various passages (self-renew more than 20 passages). Scalebar: 9000um.

Supplemental Figure 2. CUP#96 cell growth. A) Panel of brightfield images acquired every 24h for 10 days, in blue the mask used for the object area measurements. **B)** Growth curve obtained for CUP#96 spheroid analyzing images acquired every 6 hours.

Supplemental Figure 3. CUP#55 cell growth. A) Panel of brightfield images acquired every 24h for 10 days, in blue the mask used for the object area measurements. **B)** Growth curve obtained for CUP#55 cluster analyzing images acquired every 6 hours.

Supplemental Figure 4. Relative body weight (RBW) graph. Graph showing the RBW over time of N=5 mice for CUP#96 (upper panel) and CUP#55 (lower panel) PDX models. CUP#96 PDX showed a regular RBW for the entire duration of treatments instead CUP#55 PDX were sacrificed after 14 days due to cachexia induced by the tumor.

Supplemental Figure 5. FGFR2 genomic alterations in AACR GENIE (A) and MSK-IMPACT (B) cancer types with frequency > 3%. Cancers of unknown primary were tested for genomic alterations in Zehir et al study (Zehir et al., 2017) and AACR project GENIE (Consortium, 2017). In these studies, FGR2 genomic alterations were detectable with a frequency of about 3-4%. The most frequent alterations were mutations, fusions, and amplifications.

Supplemental Figure 6. FGFR2 isoforms detection in the two cell models and a control not amplified cell line. ddPCR was used to measure the abundance of two distinct isoforms of FGFR2: FGFR2IIIb epithelial and FGFR2IIIc mesenchymal. CUP#55 and CUP#96 showed higher level of FGFR2IIIb but both expressed also the mesenchymal one suggesting an epithelial-mesenchymal transition of the cells.

Supplemental Figure 7. Viability assay of CUP#55 model exposed to different concentrations of FGFR2 inhibitors. Viability reduction of CUP#55 cell line after treatment with FGFR inhibitors (BGJ398, Ponatinib, Dovitinib) or cisplatin. Data were obtained using CellTiter-Glo Luminescent Cell Viability Assay (Promega).

Supplemental Figure 8. Cell death assessment upon treatment with FGFR2 and MEK inhibitors. Representative images of CUP#55 cells untreated or treated with BGJ398 1µM and/or trametinib 100 nM for 96h and analyzed by fluorescence microscopy after Hoechst 33342/PI staining (Magnification 400X).

References

Babina, I.S., and Turner, N.C. (2017). Advances and challenges in targeting FGFR signalling in cancer. Nat Rev Cancer *17*, 318-332.

Briasoulis, E., Fountzilas, G., Bamias, A., Dimopoulos, M.A., Xiros, N., Aravantinos, G., Samantas, E., Kalofonos, H., Makatsoris, T., Mylonakis, N.*, et al.* (2008). Multicenter phase-II trial of irinotecan plus oxaliplatin [IROX regimen] in patients with poor-prognosis cancer of unknown primary: a hellenic cooperative oncology group study. Cancer Chemother Pharmacol *62*, 277-284.

Cavazzoni, A., Alfieri, R.R., Carmi, C., Zuliani, V., Galetti, M., Fumarola, C., Frazzi, R., Bonelli, M., Bordi, F., Lodola, A.*, et al.* (2008). Dual mechanisms of action of the 5-benzylidene-hydantoin UPR1024 on lung cancer cell lines. Mol Cancer Ther *7*, 361-370.

Chaffer, C.L., and Weinberg, R.A. (2011). A perspective on cancer cell metastasis. Science *331*, 1559-1564.

Clynick, B., Dessauvagie, B., Sterrett, G., Harvey, N.T., Allcock, R.J.N., Saunders, C., Erber, W., and Meehan, K. (2018). Genetic characterisation of molecular targets in carcinoma of unknown primary. J Transl Med *16*, 185.

Consortium, A.P.G. (2017). AACR Project GENIE: Powering Precision Medicine through an International Consortium. Cancer Discov *7*, 818-831.

Ding, Y., Jiang, J., Xu, J., Chen, Y., Zheng, Y., Jiang, W., Mao, C., Jiang, H., Bao, X., Shen, Y.*, et al.* (2022). Site-specific therapy in cancers of unknown primary site: a systematic review and meta-analysis. ESMO Open *7*, 100407.

Fumarola, C., La Monica, S., Alfieri, R.R., Borra, E., and Guidotti, G.G. (2005). Cell size reduction induced by inhibition of the mTOR/S6K-signaling pathway protects Jurkat cells from apoptosis. Cell Death Differ *12*, 1344-1357.

Gatalica, Z., Xiu, J., Swensen, J., and Vranic, S. (2018). Comprehensive analysis of cancers of unknown primary for the biomarkers of response to immune checkpoint blockade therapy. Eur J Cancer *94*, 179-186.

Gross-Goupil, M., Fourcade, A., Blot, E., Penel, N., Negrier, S., Culine, S., Chaigneau, L., Lesimple, T., Priou, F., Lortholary, A.*, et al.* (2012). Cisplatin alone or combined with gemcitabine in carcinomas of unknown primary: results of the randomised GEFCAPI 02 trial. Eur J Cancer *48*, 721-727.

Hainsworth, J.D., Daugaard, G., Lesimple, T., Hubner, G., Greco, F.A., Stahl, M.J., Buschenfelde, C.M., Allouache, D., Penel, N., Knoblauch, P.*, et al.* (2015). Paclitaxel/carboplatin with or without belinostat as empiric first-line treatment for patients with carcinoma of unknown primary site: A randomized, phase 2 trial. Cancer *121*, 1654-1661.

Hayashi, H., Takiguchi, Y., Minami, H., Akiyoshi, K., Segawa, Y., Ueda, H., Iwamoto, Y., Kondoh, C., Matsumoto, K., Takahashi, S.*, et al.* (2020). Site-Specific and Targeted Therapy Based on Molecular Profiling by Next-Generation Sequencing for Cancer of Unknown Primary Site: A Nonrandomized Phase 2 Clinical Trial. JAMA Oncol *6*, 1931-1938.

Huebner, G., Link, H., Kohne, C.H., Stahl, M., Kretzschmar, A., Steinbach, S., Folprecht, G., Bernhard, H., Al-Batran, S.E., Schoffski, P.*, et al.* (2009). Paclitaxel and carboplatin vs gemcitabine and vinorelbine in patients with adeno- or undifferentiated carcinoma of unknown primary: a randomised prospective phase II trial. Br J Cancer *100*, 44-49.

Izawa-Ishiguro, A.R., Sridharan, R., Wun, C., Sami, T.J., and Heller, D.A. (2022). Abstract 302: MEKi-FGFRi combination nanoparticles for use against KRASmt/FGFR-compensatory lung tumors. Cancer Research *82*, 302-302.

Janik, K., Popeda, M., Peciak, J., Rosiak, K., Smolarz, M., Treda, C., Rieske, P., Stoczynska-Fidelus, E., and Ksiazkiewicz, M. (2016). Efficient and simple approach to in vitro culture of primary epithelial cancer cells. Biosci Rep *36*.

Katoh, M. (2008). Cancer genomics and genetics of FGFR2 (Review). Int J Oncol *33*, 233-237.

Kodack, D.P., Farago, A.F., Dastur, A., Held, M.A., Dardaei, L., Friboulet, L., von Flotow, F., Damon, L.J., Lee, D., Parks, M.*, et al.* (2017). Primary Patient-Derived Cancer Cells and Their Potential for Personalized Cancer Patient Care. Cell Rep *21*, 3298-3309.

Krikelis, D., Pentheroudakis, G., Goussia, A., Siozopoulou, V., Bobos, M., Petrakis, D., Stoyianni, A., Golfinopoulos, V., Cervantes, A., Ciuleanu, T.*, et al.* (2012). Profiling immunohistochemical expression of

NOTCH1-3, JAGGED1, cMET, and phospho-MAPK in 100 carcinomas of unknown primary. Clin Exp Metastasis *29*, 603-614.
La Monica, S., Galetti, M., Alfieri, R.R., Cavazzoni, A., Ardizzoni, A., Tiseo, M., Capelletti, M., Goldoni, M., Tagliaferri, S., Mutti, A.*, et al.* (2009). Everolimus restores gefitinib sensitivity in resistant non-small cell lung cancer cell lines. Biochem Pharmacol *78*, 460-468.
Laprovitera, N., Riefolo, M., Ambrosini, E., Klec, C., Pichler, M., and Ferracin, M. (2021a). Cancer of Unknown Primary: Challenges and Progress in Clinical Management. Cancers (Basel) *13*.
Laprovitera, N., Riefolo, M., Porcellini, E., Durante, G., Garajova, I., Vasuri, F., Aigelsreiter, A., Dandachi, N., Benvenuto, G., Agostinis, F.*, et al.* (2021b). MicroRNA expression profiling with a droplet digital PCR assay enables molecular diagnosis and prognosis of cancers of unknown primary. Mol Oncol *15*, 2732-2751.
Laprovitera, N., Salamon, I., Gelsomino, F., Porcellini, E., Riefolo, M., Garonzi, M., Tononi, P., Valente, S., Sabbioni, S., Fontana, F.*, et al.* (2021c). Genetic Characterization of Cancer of Unknown Primary Using Liquid Biopsy Approaches. Front Cell Dev Biol *9*, 666156.
Lombardo, R., Tosi, F., Nocerino, A., Bencardino, K., Gambi, V., Ricotta, R., Spina, F., Siena, S., and Sartore-Bianchi, A. (2020). The Quest for Improving Treatment of Cancer of Unknown Primary (CUP) Through Molecularly-Driven Treatments: A Systematic Review. Front Oncol *10*, 533.
Pentheroudakis, G., Briasoulis, E., Kalofonos, H.P., Fountzilas, G., Economopoulos, T., Samelis, G., Koutras, A., Karina, M., Xiros, N., Samantas, E.*, et al.* (2008). Docetaxel and carboplatin combination chemotherapy as outpatient palliative therapy in carcinoma of unknown primary: a multicentre Hellenic Cooperative Oncology Group phase II study. Acta Oncol *47*, 1148-1155.
Ross, J.S., Wang, K., Gay, L., Otto, G.A., White, E., Iwanik, K., Palmer, G., Yelensky, R., Lipson, D.M., Chmielecki, J.*, et al.* (2015). Comprehensive Genomic Profiling of Carcinoma of Unknown Primary Site: New Routes to Targeted Therapies. JAMA Oncol *1*, 40-49.
SenthilKumar, G., Fisher, M.M., Skiba, J.H., Miller, M.C., Brennan, S.R., Kaushik, S., Bradley, S.T., Longhurst, C.A., Buehler, D., Nickel, K.P.*, et al.* (2020). FGFR Inhibition Enhances Sensitivity to Radiation in Non-Small Cell Lung Cancer. Mol Cancer Ther *19*, 1255-1265.
Smyth, E.C., Babina, I.S., and Turner, N.C. (2017). Gatekeeper Mutations and Intratumoral Heterogeneity in FGFR2-Translocated Cholangiocarcinoma. Cancer Discov *7*, 248-249.
Varadhachary, G.R., and Raber, M.N. (2014). Cancer of unknown primary site. N Engl J Med *371*, 757-765.
Varghese, A.M., and Saltz, L.B. (2015). Genomic Profiling of Cancers of Unknown Primary Site: The Next Steps. JAMA Oncol *1*, 541-542.
Verginelli, F., Pisacane, A., Gambardella, G., D'Ambrosio, A., Candiello, E., Ferrio, M., Panero, M., Casorzo, L., Benvenuti, S., Cascardi, E.*, et al.* (2021). Cancer of unknown primary stem-like cells model multi-organ metastasis and unveil liability to MEK inhibition. Nat Commun *12*, 2498.
Wainberg, Z.A., Enzinger, P.C., Kang, Y.K., Qin, S., Yamaguchi, K., Kim, I.H., Saeed, A., Oh, S.C., Li, J., Turk, H.M.*, et al.* (2022). Bemarituzumab in patients with FGFR2b-selected gastric or gastro-oesophageal junction adenocarcinoma (FIGHT): a randomised, double-blind, placebo-controlled, phase 2 study. Lancet Oncol *23*, 1430-1440.
Warner, E., Goel, R., Chang, J., Chow, W., Verma, S., Dancey, J., Franssen, E., Dulude, H., Girouard, M., Correia, J.*, et al.* (1998). A multicentre phase II study of carboplatin and prolonged oral etoposide in the treatment of cancer of unknown primary site (CUPS). Br J Cancer *77*, 2376-2380.
Zehir, A., Benayed, R., Shah, R.H., Syed, A., Middha, S., Kim, H.R., Srinivasan, P., Gao, J., Chakravarty, D., Devlin, S.M.*, et al.* (2017). Mutational landscape of metastatic cancer revealed from prospective clinical sequencing of 10,000 patients. Nat Med *23*, 703-713.

Figure 1

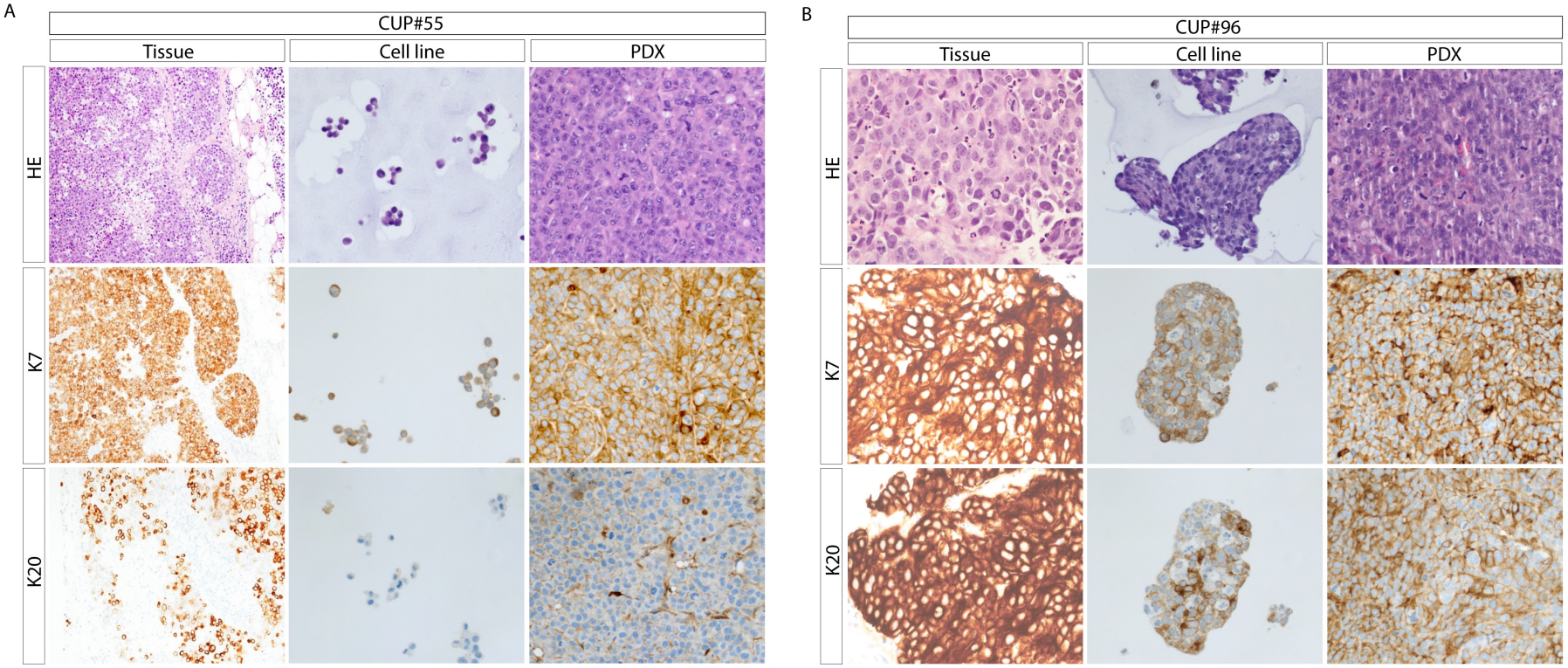
A
CUP#55
Tissue
Cell line
PDX
HE
K7
K20
B
CUP#96
Tissue
Cell line
PDX
HE
K7
K20

Figure 2

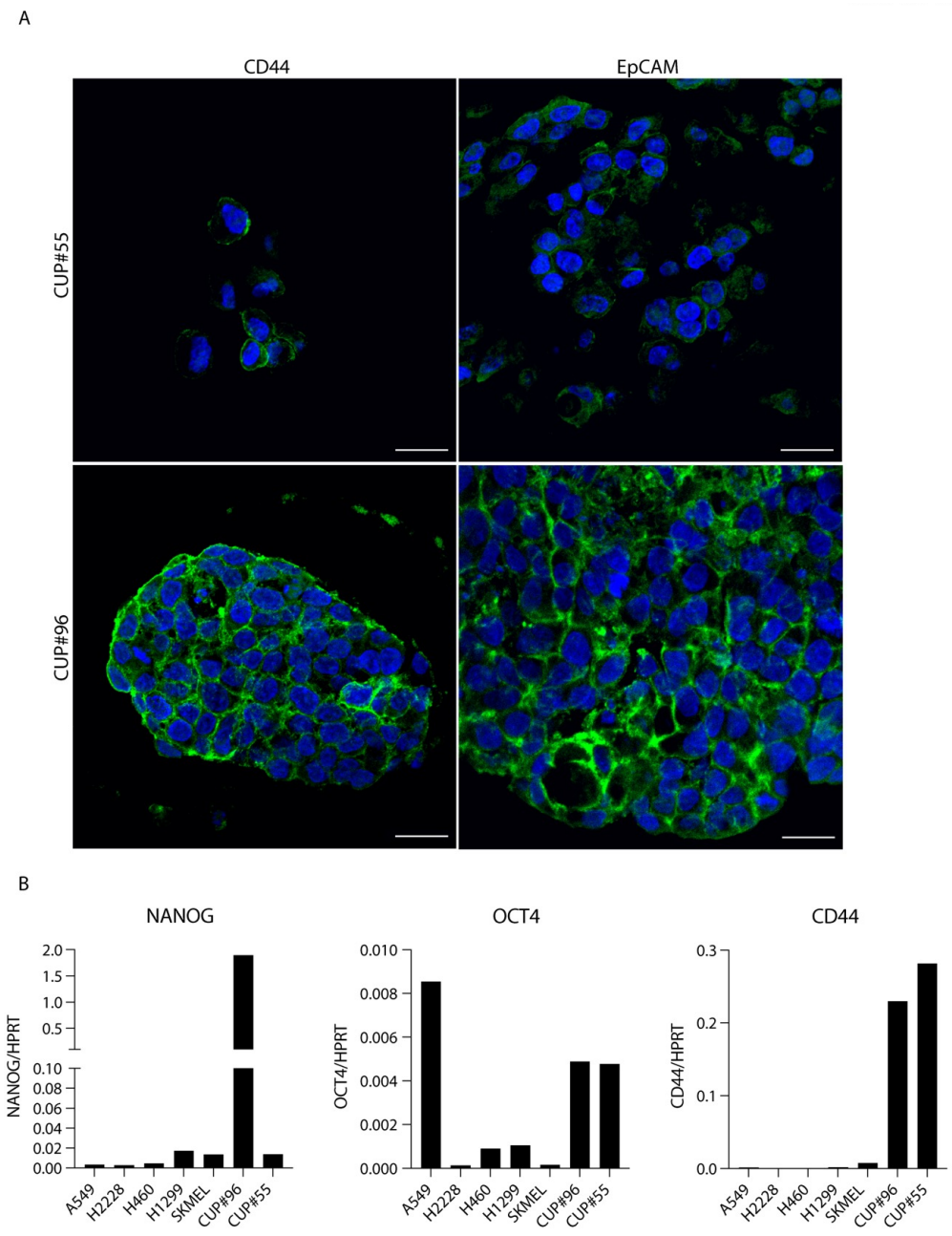
A
CD44
EpCAM
CUP#55
CUP#96
B
NANOG
OCT4
CD44
NANOG/HPRT
OCT4/HPRT
CD44/HPRT
2.0
1.5
1.0
0.5
0.10
0.08
0.06
0.04
0.02
0.00
0.010
0.008
0.006
0.004
0.002
0.000
0.3
0.2
0.1
0.0
A549
H2228
H460
H1299
SKMEL
CUP#96
CUP#55

Figure 3

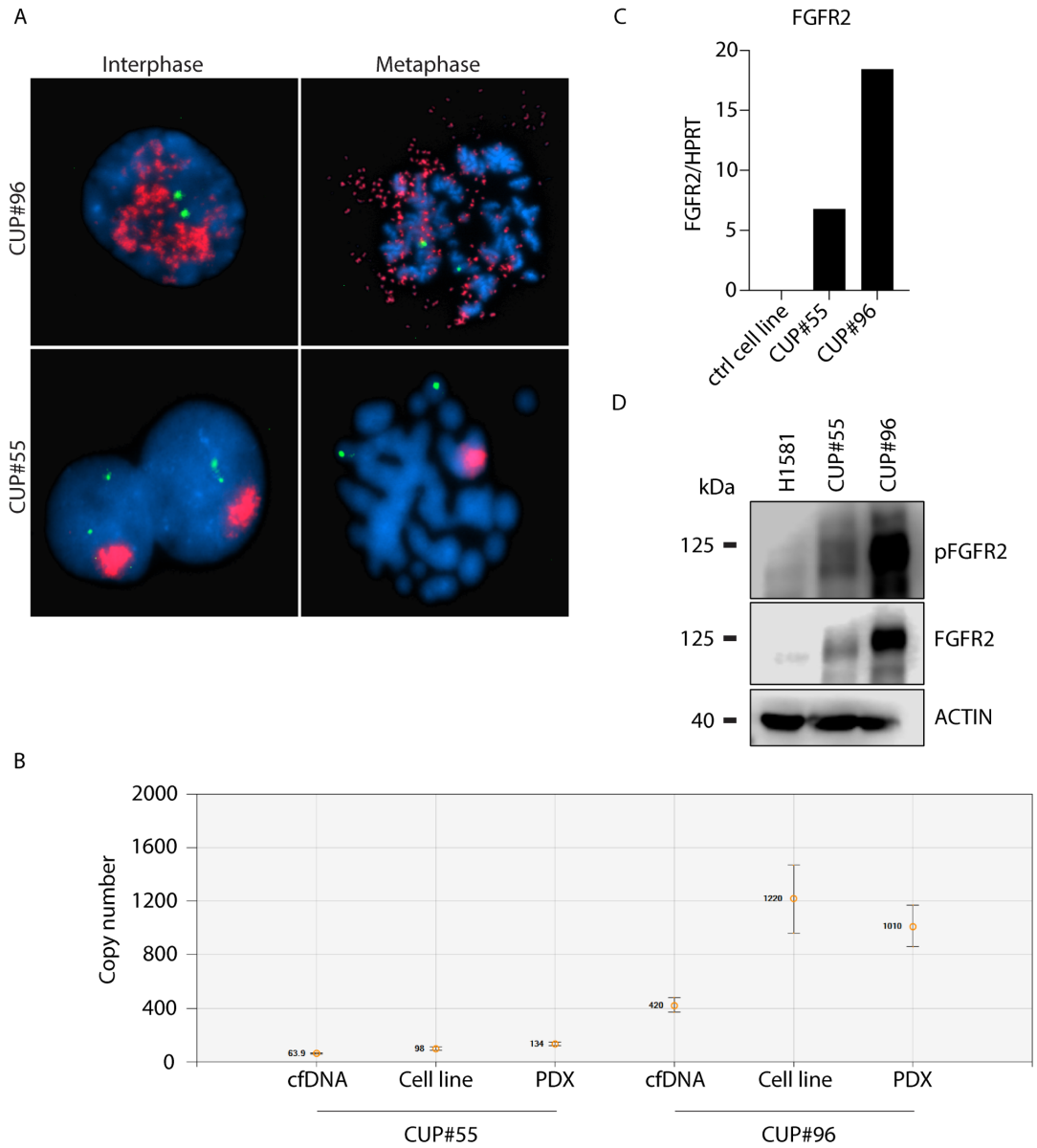
A
Interphase
Metaphase
CUP#96
CUP#55
C
FGFR2
FGFR2/HPRT
20
15
10
5
0
ctrl cell line
CUP#55
CUP#96
D
kDa
H1581
CUP#55
CUP#96
125
pFGFR2
125
FGFR2
40
ACTIN
B
Copy number
2000
1600
1200
800
400
0
63.9
98
134
420
1220
1010
cfDNA
Cell line
PDX
cfDNA
Cell line
PDX
CUP#55
CUP#96

Figure 4

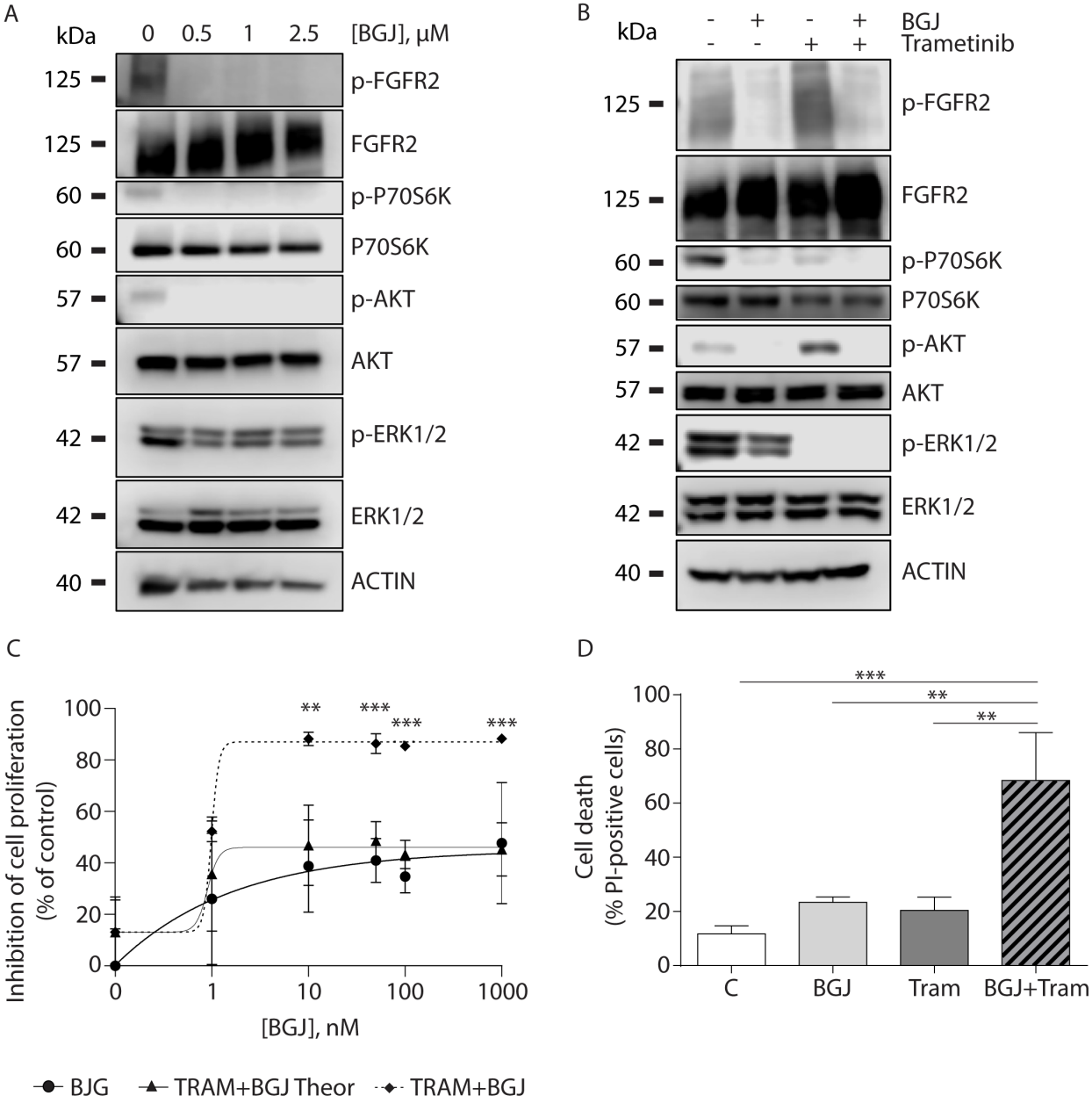
A
kDa
0
0.5
1
2.5
[BGJ], μM
125
p-FGFR2
125
FGFR2
60
p-P70S6K
60
P70S6K
57
p-AKT
57
AKT
42
p-ERK1/2
42
ERK1/2
40
ACTIN
B
kDa
BGJ
Trametinib
125
p-FGFR2
125
FGFR2
60
p-P70S6K
60
P70S6K
57
p-AKT
57
AKT
42
p-ERK1/2
42
ERK1/2
40
ACTIN
C
Inhibition of cell proliferation (% of control)
[BGJ], nM
BJG
TRAM+BGJ Theor
TRAM+BGJ
D
Cell death (% PI-positive cells)
C
BGJ
Tram
BGJ+Tram

Figure 5

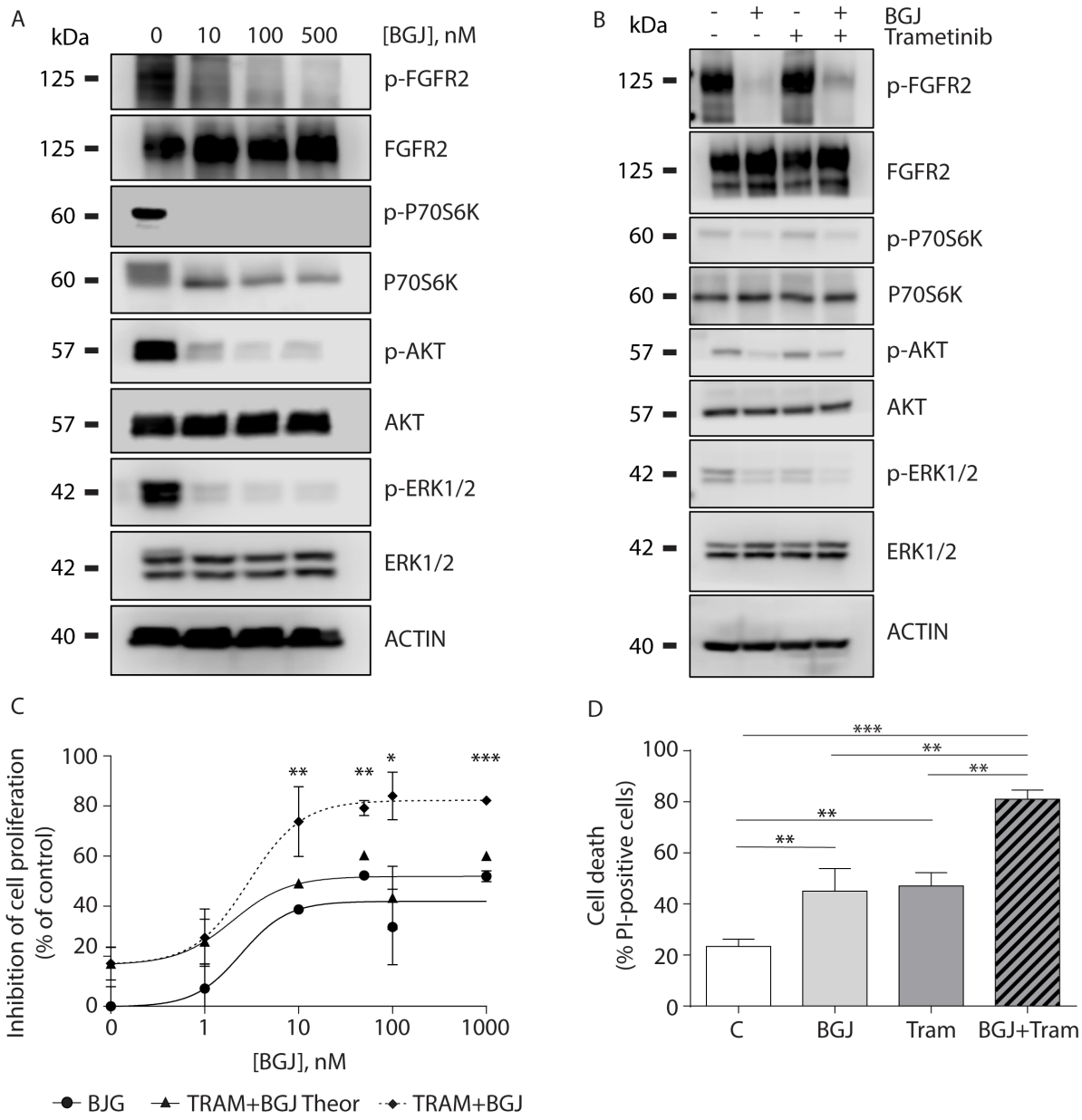
A
kDa
0
10
100
500
[BGJ], nM
125
p-FGFR2
125
FGFR2
60
p-P70S6K
60
P70S6K
57
p-AKT
57
AKT
42
p-ERK1/2
42
ERK1/2
40
ACTIN
B
kDa
BGJ
Trametinib
125
p-FGFR2
125
FGFR2
60
p-P70S6K
60
P70S6K
57
p-AKT
57
AKT
42
p-ERK1/2
42
ERK1/2
40
ACTIN
C
Inhibition of cell proliferation
(% of control)
[BGJ], nM
BJG
TRAM+BGJ Theor
TRAM+BGJ
D
Cell death
(% PI-positive cells)
C
BGJ
Tram
BGJ+Tram

Figure 6

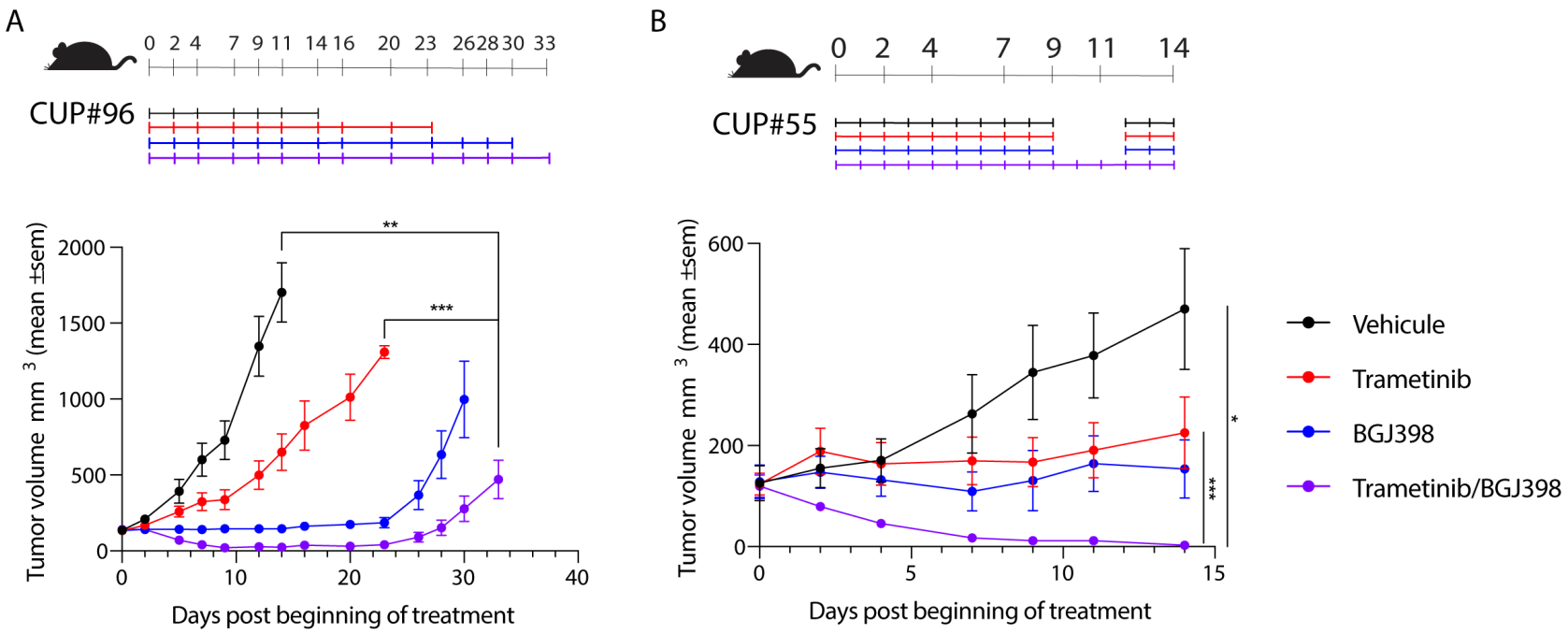
A
0 2 4 7 9 11 14 16 20 23 26 28 30 33
CUP#96
Tumor volume mm 3 (mean ±sem)
2000
1500
1000
500
0
**
***
0
10
20
30
40
Days post beginning of treatment
B
0 2 4 7 9 11 14
CUP#55
Tumor volume mm 3 (mean ±sem)
600
400
200
0
*
***
0
5
10
15
Days post beginning of treatment
Vehicule
Trametinib
BGJ398
Trametinib/BGJ398

Supplementary Figure 1

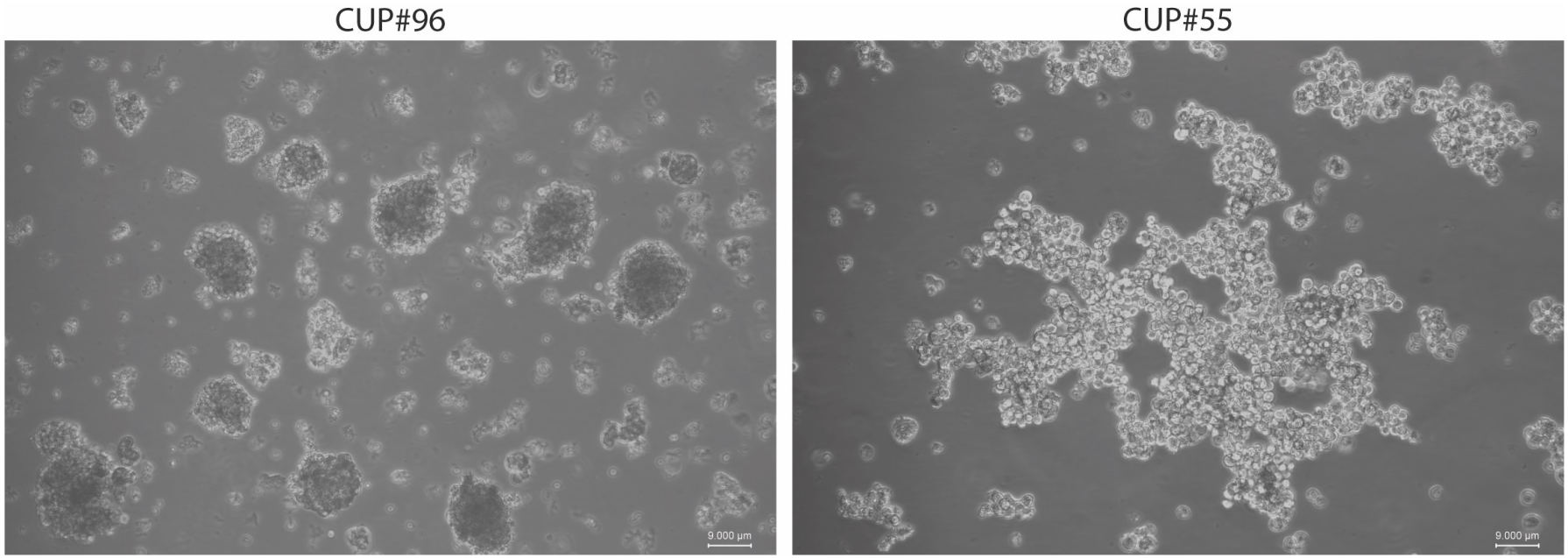

Supplementary Figure 2

A CUP#96

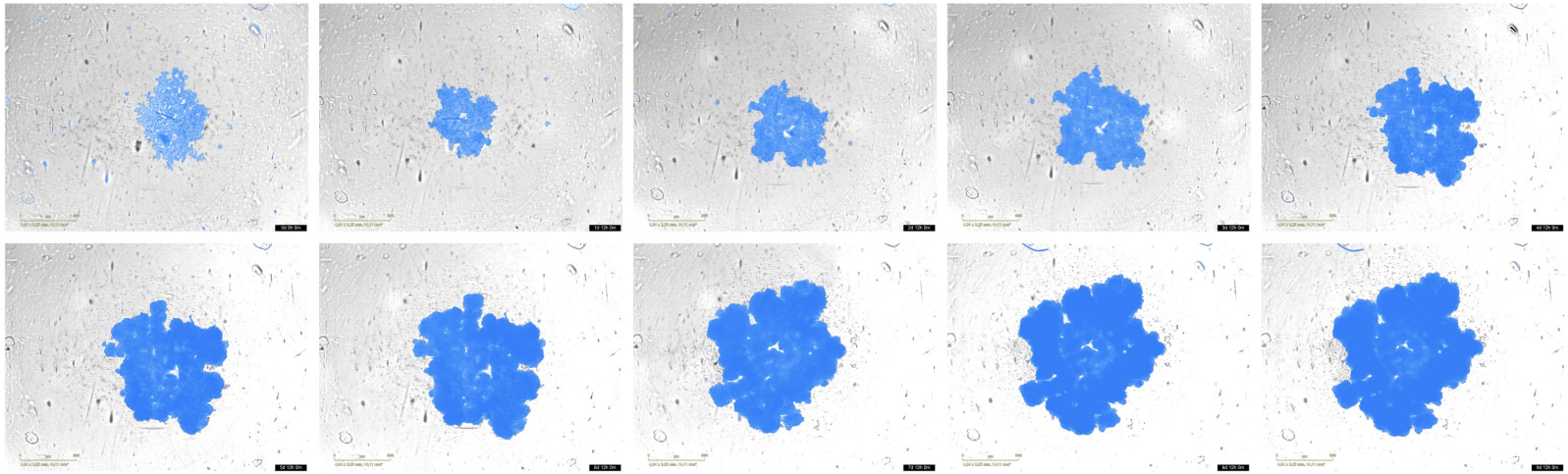

B

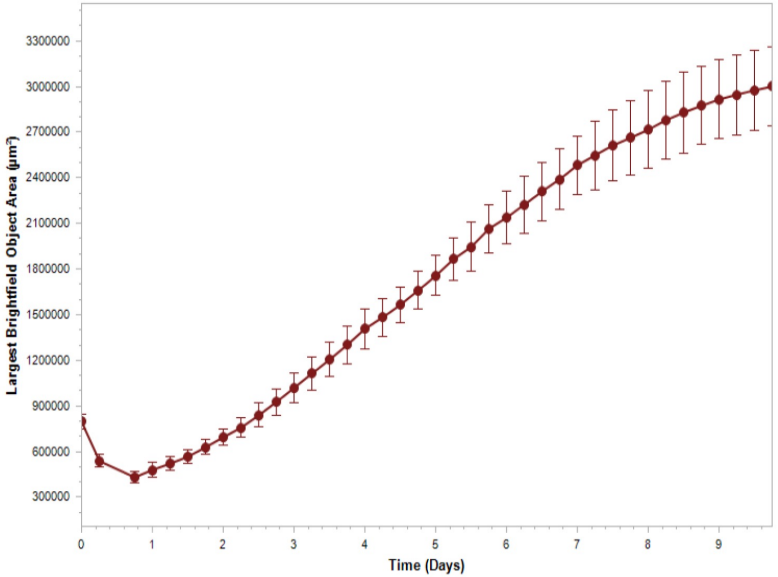

Supplementary Figure 3

A CUP#55

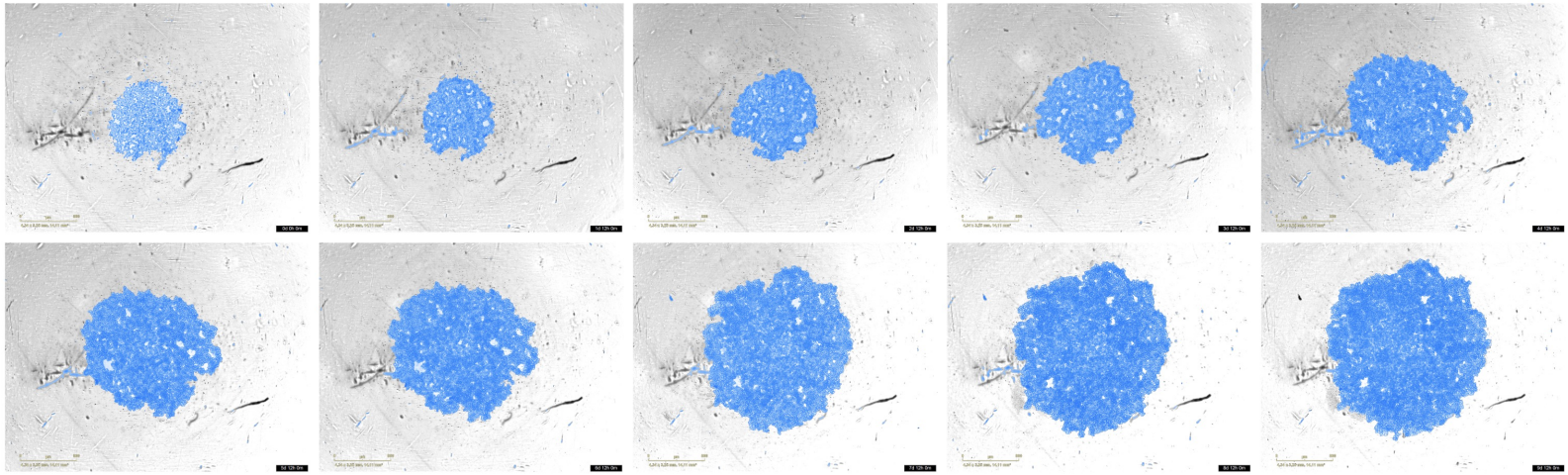

B

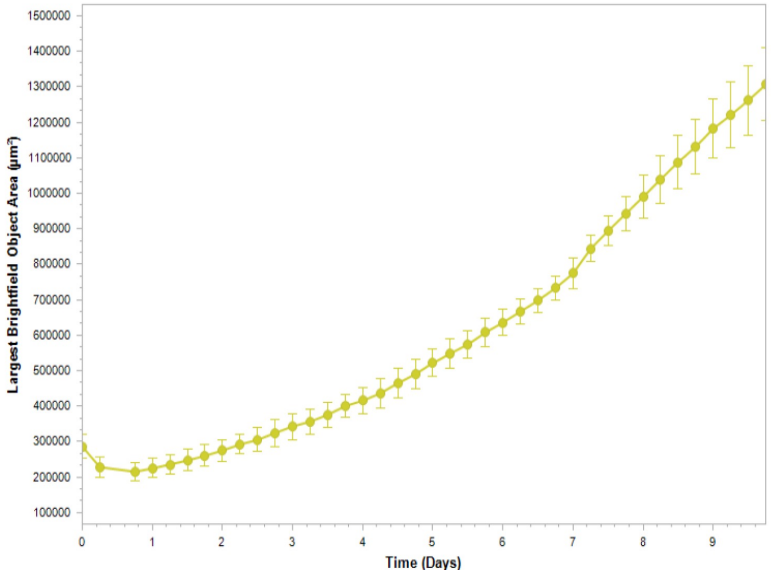

Supplementary Figure 4

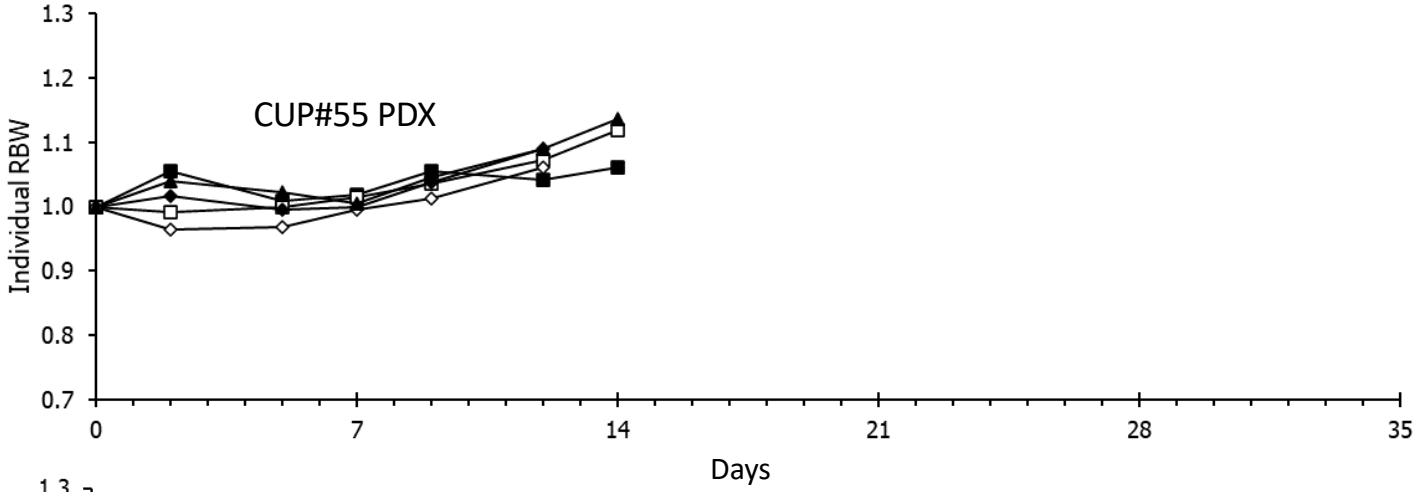

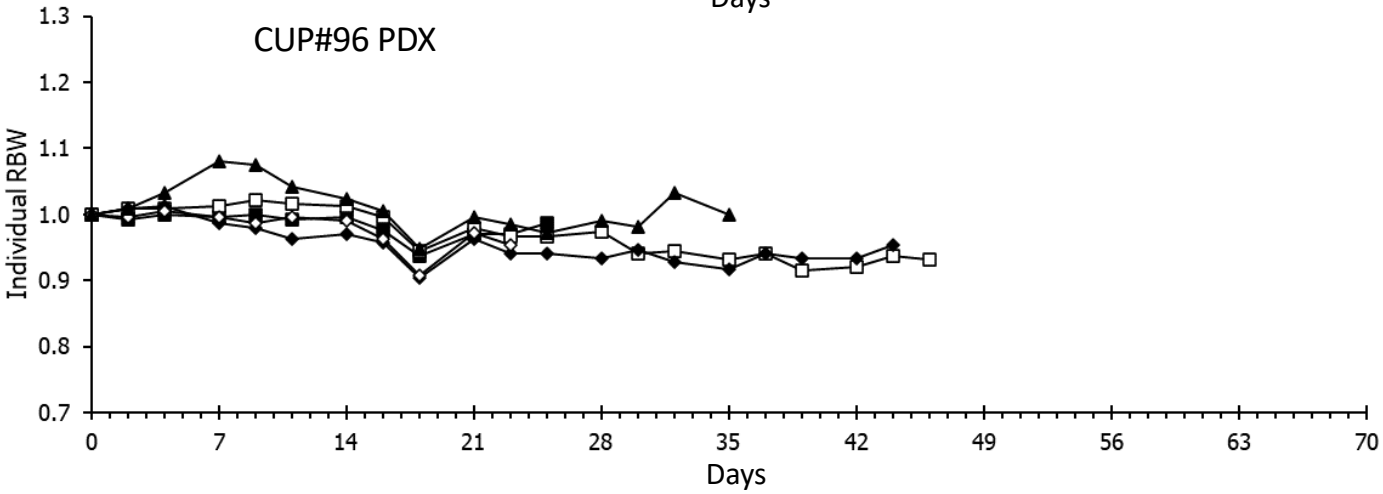

RBW= relative body weight

Supplementary Figure 5

A

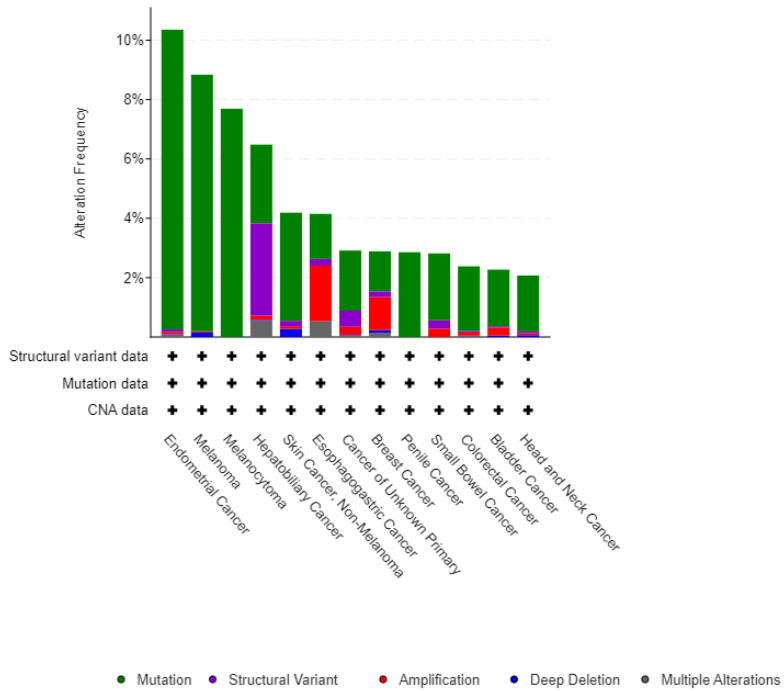

B

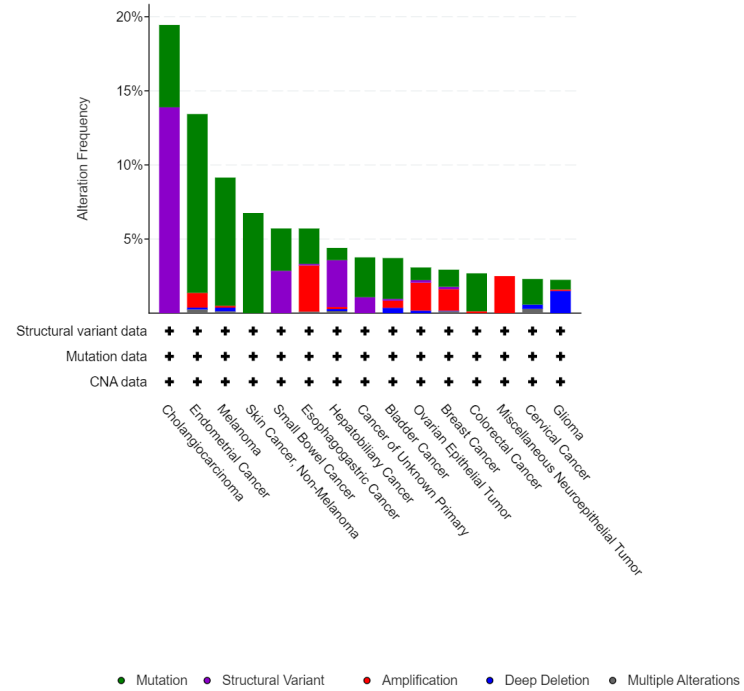

Supplementary Figure 6

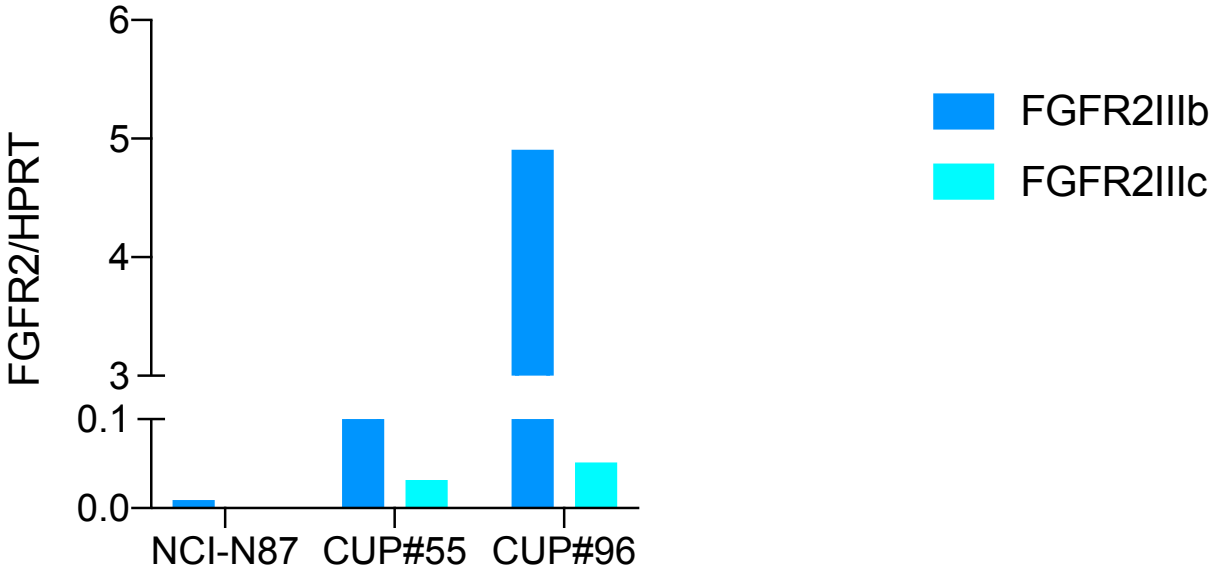

Supplementary Figure 7

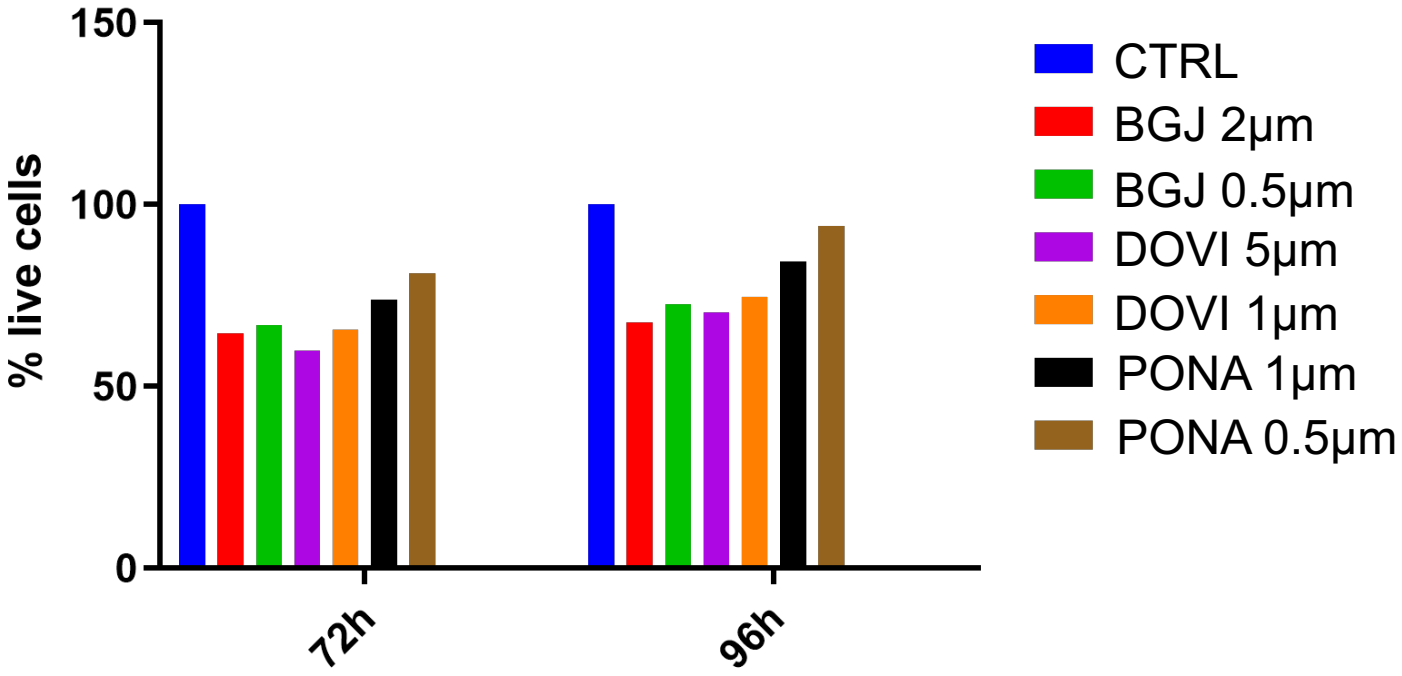

Supplementary Figure 8

CUP#55

Control

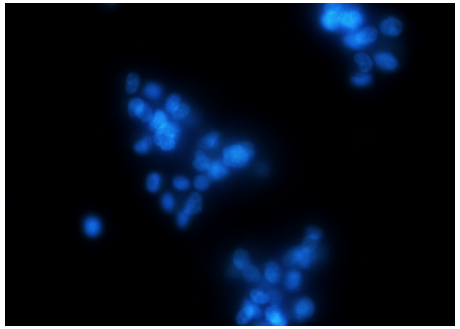

BGJ

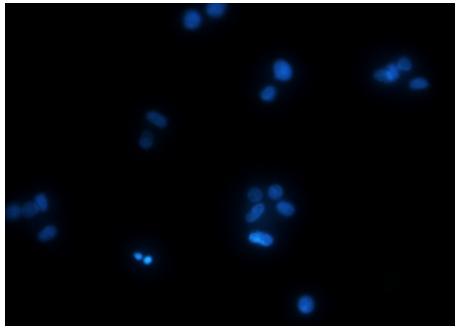

Tram

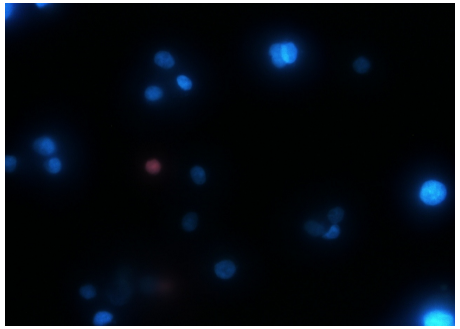
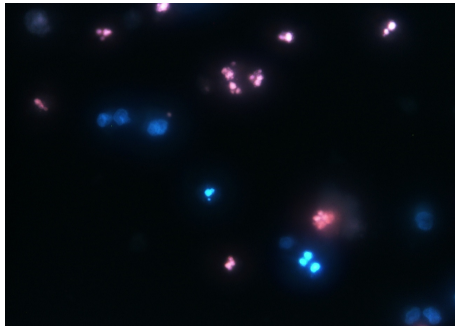
BGJ+Tram